CRISPR-Mediated Genomic Deletion of *Sox2* in the Axolotl Shows a Requirement in Spinal Cord Neural Stem Cell Amplification during Tail Regeneration

Ji-Feng Fei,[1] Maritta Schuez,[1] Akira Tazaki,[1] Yuka Taniguchi,[1] Kathleen Roensch,[1] and Elly M. Tanaka[1,*]

[1]DFG Center for Regenerative Therapies, Dresden (CRTD), Technische Universität Dresden, Dresden 01307, Germany
*Correspondence: elly.tanaka@crt-dresden.de

SUMMARY

The salamander is the only tetrapod that functionally regenerates all cell types of the limb and spinal cord (SC) and thus represents an important regeneration model, but the lack of gene-knockout technology has limited molecular analysis. We compared transcriptional activator-like effector nucleases (TALENs) and clustered regularly interspaced short palindromic repeats (CRISPRs) in the knockout of three loci in the axolotl and find that CRISPRs show highly penetrant knockout with less toxic effects compared to TALENs. Deletion of *Sox2* in up to 100% of cells yielded viable F0 larvae with normal SC organization and ependymoglial cell marker expression such as GFAP and ZO-1. However, upon tail amputation, neural stem cell proliferation was inhibited, resulting in spinal-cord-specific regeneration failure. In contrast, the mesodermal blastema formed normally. *Sox3* expression during development, but not regeneration, most likely allowed embryonic survival and the regeneration-specific phenotype. This analysis represents the first tissue-specific regeneration phenotype from the genomic deletion of a gene in the axolotl.

INTRODUCTION

The molecular study of regeneration in animals such as the salamander serves as an important basis for understanding the limited regenerative abilities of other animals. The salamander is the only tetrapod where full cellular reconstitution of a lesioned spinal cord occurs and where the adult limb functionally regenerates all constituent tissues, and it therefore plays particular significance in understanding regenerative ability and how it may be improved (Kragl et al., 2008, 2009; Simon and Tanaka, 2013; Tanaka and Ferretti, 2009). The relevance of salamander regeneration to mammals was highlighted in an analysis of mouse digit tip regeneration, which showed that the molecular factors mediating tissue interactions between nerve and skin were similar to those first identified during salamander limb regeneration (Takeo et al., 2013). Furthermore, the extensive skin-regenerative capacities of the spiny mouse were shown to utilize an extracellular matrix (ECM) environment similar to those defined for salamander limb regeneration, suggesting that the implementation of certain ECM-expression programs is associated with deep regenerative ability (Seifert et al., 2012). Therefore, deepening our understanding of the molecular programs underlying the regenerative response in salamanders is an important endeavor.

Targeted overexpression of genes via electroporation, viral transduction, or transgenesis as well as knockdown of protein expression via electroporation morpholinos, respectively, has been an important means of molecularly analyzing regeneration in the axolotl (Echeverri and Tanaka, 2005; Kawakami et al., 2006; Khattak et al., 2013; Mercader et al., 2005; Roy et al., 2000; Whited et al., 2013). However, the lack of stable genomic knockout in the axolotl had limited molecular studies. Recently, exciting progress has been made on genome editing using zinc-finger nucleases, transcriptional activator-like effector nucleases (TALENs), and clustered regularly interspaced short palindromic repeat (CRISPR) systems (for review, see Gaj et al., 2013). With these methods, highly efficient gene knockout or homologous gene knockin has been achieved in a variety of species including vertebrates such as *Xenopus*, zebrafish, and rodents. Studies implementing TALENs in *Xenopus* reported that targeted deletions reach efficiencies up to 100% of alleles (Lei et al., 2012; Suzuki et al., 2013). The effectiveness of TALENs was also recently demonstrated in the ribbed Iberian newt, *Pleurodeles waltl* (Hayashi et al., 2014). These results indicate that TALENs are a highly versatile system for targeting deletions and gene insertions into vertebrate genomes.

Recently, an alternative method of genome editing was described, based on nucleases of the bacterial antiphage "immune" system, CRISPR (for review, see Gaj et al., 2013; Mali et al., 2013a). Several groups engineered a two-component system for genome editing in which a single guide RNA (gRNA) was coexpressed with the *Cas9* gene (Cong et al., 2013; Jinek et al., 2012; Mali et al., 2013b). This two-component system resulted in highly efficient generation of indels at the target site. In human embryonic stem cells, depending on the target, 1%–34% of expressing cells showed a deletion of at least one targeted allele. The method has also been used to demonstrate the possibility

CrossMark

of generating genomic deletions in several model systems, including the axolotl (Blitz et al., 2013; Flowers et al., 2014; Hwang et al., 2013; Nakayama et al., 2013).

In most vertebrate models, mRNAs encoding TALENs and CRISPRs have been injected into the egg to generate genomic deletions from the beginning of development. Since regeneration is a late event, a question is whether this means of knocking out genes can be applied to studying specific cell types during regeneration or whether more sophisticated methods to induce knockouts later in development will be necessary. Here, we investigated the utility of the CRISPR system to knock out a key neural stem gene, *Sox2*, with the aim to study its role in the regenerating spinal cord. SOX2 is an SRY-related high-mobility group box transcription factor that supports embryonic pluripotency (Avilion et al., 2003), and it later plays a key role in the development, maintenance, and expansion of neural stem/progenitor cells (Bylund et al., 2003; Favaro et al., 2009; Takemoto et al., 2011). In addition, *Sox2* is required to maintain the proliferative progenitor pool in various adult epithelia (Arnold et al., 2011; Que et al., 2009). In the axolotl, SOX2 is expressed in the mature spinal cord and in cultured spinal cord neurospheres that harbor multipotent neural stem cells that reconstitute the different spinal cord cell types (McHedlishvili et al., 2012; Tapia et al., 2012). The molecular factors that support the rapid expansion and self-renewal of neural stem cells during spinal cord regeneration after tail amputation were unknown. Here, we show by the CRISPR-mediated genomic deletion of *Sox2* that axolotls harboring up to 100% *Sox2* deleted cells survive embryonic development to generate larvae with a normal spinal cord cell complement and neuronal number. Morpholino knockdown of SOX2 in the embryo confirms lack of embryonic lethality. Upon tail amputation, however, the spinal cord cells do not increase their proliferation, resulting in defective expansion and an overall lack of spinal cord in the regenerating tail. Expression analysis of *Sox3* shows overlapping expression with *Sox2* during neural tube development, but not regeneration, rationalizing the spinal cord regeneration-specific phenotype. Despite severe defects in the regenerating spinal cord, the regenerative epidermis and the mesenchymal blastema form normally in *Sox2*-CRISPR animals.

RESULTS

CRISPRs Mediate More Efficient, Less Toxic Gene Knockout Than TALENs in Axolotl

Germline-Transmitted Knockout of a GFP-Transgene

To determine if TALENs and CRISPRs can mediate efficient gene deletions, we initially chose to knock out a genomically inserted *GFP*-transgene in our germline-transgenic

GFP-axolotl strain (Sobkow et al., 2006) to have an easy readout for successful gene knockout. Two pairs of *GFP*-TALENs and two pairs of CRISPR *GFP*-gRNAs in corresponding regions were designed according to published protocols (Cermak et al., 2011; Cong et al., 2013; Mali et al., 2013b) (Figures 1A–1A″; see the Experimental Procedures). We injected the TALEN mRNAs (mixture of left- and right-arm mRNAs) or CRISPR RNAs (mixture of *Cas9* mRNA and *GFP*-gRNA) into freshly laid axolotl embryos with the aim of eliciting knockout of the genomic *GFP* as early as possible. In the egg injection experiments, we titrated the amount of injected TALEN (Table S1 available online) and CRISPR (Table S2) RNAs and found that the CRISPR RNAs were significantly less toxic to embryos (evaluated at 10 days postinjection) (Tables S1 and S2). We next assessed the efficiency of genomic modification. Injections of *GFP*-TALEN pair #1 or #3 mRNA, but not control TALENs (#1 left-arm plus #3 right-arm mRNAs), into embryos resulted in 24%–34% of the larvae showing a visible loss or reduction of GFP expression in at least some tissue/body cells in the resulting larvae (Figures 1B and C; Table S3). GFP expression was markedly reduced in the normally strongly expressing muscle, as confirmed on histological cross-sections (Figure 1C). The genomic generation of indels was confirmed by genomic PCR (Figure 1D). Animals modified by *GFP*-TALENs #1 and #3 were grown to adulthood, and both showed germline transmission of the *GFP* deletion with a representative transmission frequency of 56%.

In comparison to TALENs, injection of CRISPR *GFP*-gRNA #3 generated *GFP* deletions at a higher penetrance and efficiency. A total of 55% of injected animals showed at least some loss of GFP expression. Of the animals showing modification, 60% showed greater than 50% of cells lacking GFP expression (Table S3; Figures 1E–1F″). Control CRISPR *Tyrosinase(Tyr)*-gRNA did not yield knockdown of GFP expression (Figures 1G–1G″). Cryosections confirmed the loss of GFP expression in *GFP*-gRNA#3-injected, but not control *Tyr*-gRNA#1-injected, animals at the cellular level (Figure 1H). Finally, PCR cloning and sequencing of genomic DNA isolated from individual injected animals showed a large proportion of clones (cells) with deletions at the target *GFP* sequence (Figure 1I). Control-injected embryos showed no modification of the *GFP* locus. Germline transmission of CRISPRs is still to be determined. In summary, our results showed that *GFP*-TALENs and *GFP*-CRISPRs can successfully modify the *GFP*-transgene, with CRISPR mediating more efficient, less toxic effects.

Efficient Knockout of the Endogenous Tyrosinase Gene

To assess the effectiveness of TALENs and CRISPRs on an endogenous gene, we first chose the axolotl *Tyrosinase* (*Tyr*) gene as it is a nonessential gene whose knockout gives a clear, pigmentation defect. To knock out *Tyr*, two pairs of *Tyr*-TALENS (#3 and #4) and three CRISPR gRNAs

Figure 1. Deletions in a *GFP*-Transgene in the Axolotl Genome via TALEN or CRISPR Injections

(A–A'') TALENs (green) and CRISPR gRNAs (red) were designed to target the *GFP* sequence and injected into one-cell-stage eggs.

(B) Representative axolotl larvae that received *GFP*-TALEN #3 in which half of the body (red arrow compared to green arrow) has lost GFP expression. Control (*GFP*-TALEN #1 left-arm plus #3 right-arm mRNAs) injection showed bilaterally symmetric GFP expression (green arrows). Scale bar, 2 mm.

(C) Tail cross-sections from *GFP*-TALEN #3 knockdown versus control knockdown animals counterstained for DAPI and muscle-specific myosin heavy chain (MHC) immunostaining. GFP fluorescence signal is missing in muscle cells of the *GFP*-TALEN section, but not in a comparable region of the control animal. Region of interest is shown and zoomed by the white box. Scale bar, 200 μm.

(Figure 2A) were assessed by injection of RNAs into embryos and examined 13 days postinjection (Table S4). A total of 60% of animals injected with *Tyr*-TALEN #4 mRNA showed at least some loss of pigment in the body (Figures 2B and 2B′). In comparison, the most efficient CRISPR *Tyr*-gRNA#1 yielded 99% of animals showing loss in pigment, with 86% showing apparently complete loss of pigment (Table S4; Figures 2E and 2E′). Animals injected with control TALEN (left arm of *Tyr*-TALEN #4) and *GFP*-gRNA#3 showed no loss in pigmentation (Figures 2C, 2C′, 2F, and 2F′). Again, PCR amplification, cloning, and sequencing of the target *Tyr* sequence showed a higher rate of deletions from *Tyr*-CRISPR (Figure 2G) when compared to *Tyr*-TALEN (Figure 2D). Our results show that for two independent gene-knockout trials, CRISPRs showed a higher frequency and penetrance of gene knockdown with less animal lethality compared to TALENs.

Axolotls Harboring CRISPR-Mediated Deletions in *Sox2* Show Normal Size and Organization of the Spinal Cord during Development

Given the higher success rate with CRISPRs, we sought to determine the role of *Sox2* in axolotl spinal cord development and regeneration by the generation of CRISPR-mediated gene deletions. In axolotls, SOX2 expression was associated with neural stem cells that have the ability to clonally reconstitute spinal cord cell types during tail regeneration (McHedlishvili et al., 2012). In order to effectively disrupt the protein-coding sequence of *Sox2*, seven CRISPR targeting sites were selected as close as possible to the translational start codon (Figures 3A and 3B). *Sox2*-CRISPR RNAs were injected into fertilized eggs at the single-cell stage and analyzed 13 days postinjection. Of the seven *Sox2*-gRNAs designed, two of them, *Sox2*-gRNA#2 targeting the N-terminal region and *Sox2*-gRNA#4 targeting the middle of the sequence, gave identical, penetrant phenotypes described below, while a smaller proportion of *Sox2*-gRNA#5-injected animals gave a milder version of

the phenotype and the other four *Sox2*-gRNAs gave no apparent phenotype. Of 487 eggs injected with *Sox2*-gRNA#2, 403 survived, hatched, and grew to normal sizes. Upon closer visual inspection of behavior, 274 (68%) showed a curved body (Figure 3C) when swimming, and many appeared to have excess blood in the olfactory bulb area (Figure 3C′, red arrow). The same phenotype was observed from *Sox2*-gRNA#4-injected animals (Figures 3E and 3E′). This phenotype was never observed in the *GFP*-gRNA#1-injected animals (Figures 3D, 3D′, 3F, and 3F′). Immunohistological examination of the olfactory bulb confirmed a severe reduction in SOX2-positive cells at the lumen of the olfactory bulb and a general loss of cell number (Figure S1A). The observation of identical phenotypes from two different *Sox2*-gRNAs, combined with the absence of the phenotype in all animals injected with *GFP* and *Tyrosinase* gRNAs, indicates that the phenotypes are specific to *Sox2* deletion and not due to off-target effects.

The genetic knockout of *Sox2* in mice results in preimplantation lethality (Avilion et al., 2003), and therefore, the survival through embryonic development was surprising, although knockdown of *Sox2* by morpholino in amphibian or fish has not been reported. We therefore analyzed the penetrance of CRISPR-mediated *Sox2* deletions within individual animals at two developmental stages: embryonic stage 15 (neural plate stage) and day 13 larvae. At stage 15, when there was no scorable phenotype, injected animals were randomly selected and genotyped by PCR. Among this cohort, 4 out of 11 animals yielded 100% of cloned inserts with deletions in *Sox2*, indicating that animals can survive to stage 15 with what appears to be complete penetrance of *Sox2* deletion (Figure S1B). Day 13 larvae could be phenotypically sorted based on the curved-body phenotype (68% of total). Genotyping of the curved-body animals showed 8 out of 11 animals with 100% of clones containing deletions in *Sox2* (Figures 3G and

(D) Analysis of genomic target site in two individuals injected with *GFP*-TALEN #3 by PCR amplification and sequencing of clones. A total of 9 out of 15 clones showed deletions or deletions plus insertions in the genomic sequence, reflecting a high rate of genome modification in the cells.

(E) Representative axolotl larva that received CRISPR *GFP*-gRNA#3 in which >50% of cells have lost GFP expression.

(E′) GFP expression is reduced throughout the body.

(E″) High-magnification view of tail tissue. Only a few remaining GFP cells are visible (red arrow).

(F–F″) Another representative axolotl larva with extensive knockout in 50% of the body.

(G–G″) Injection of CRISPR gRNAs targeting the axolotl *Tyrosinase* (*Tyr*) gene as a control shows no knockdown of the *GFP*-transgene. Scale bars represent 1 mm in (E) and 500 μm in (E″).

(H) Tail cross-sections from CRISPR *GFP* knockdown versus control *Tyrosinase* knockdown animals counterstained for DAPI and MHC immunostaining. GFP fluorescence signal is missing in most cells of the *GFP*-gRNA#3 section. Scale bars, 100 μm.

(I) Analysis of genomic target site in two individuals injected with *GFP*-gRNA#3 by PCR amplification and sequencing of clones. In both samples, all 12 clones showed deletions or deletions plus insertions in the genomic sequence, reflecting a high rate of genome modification in the cells.
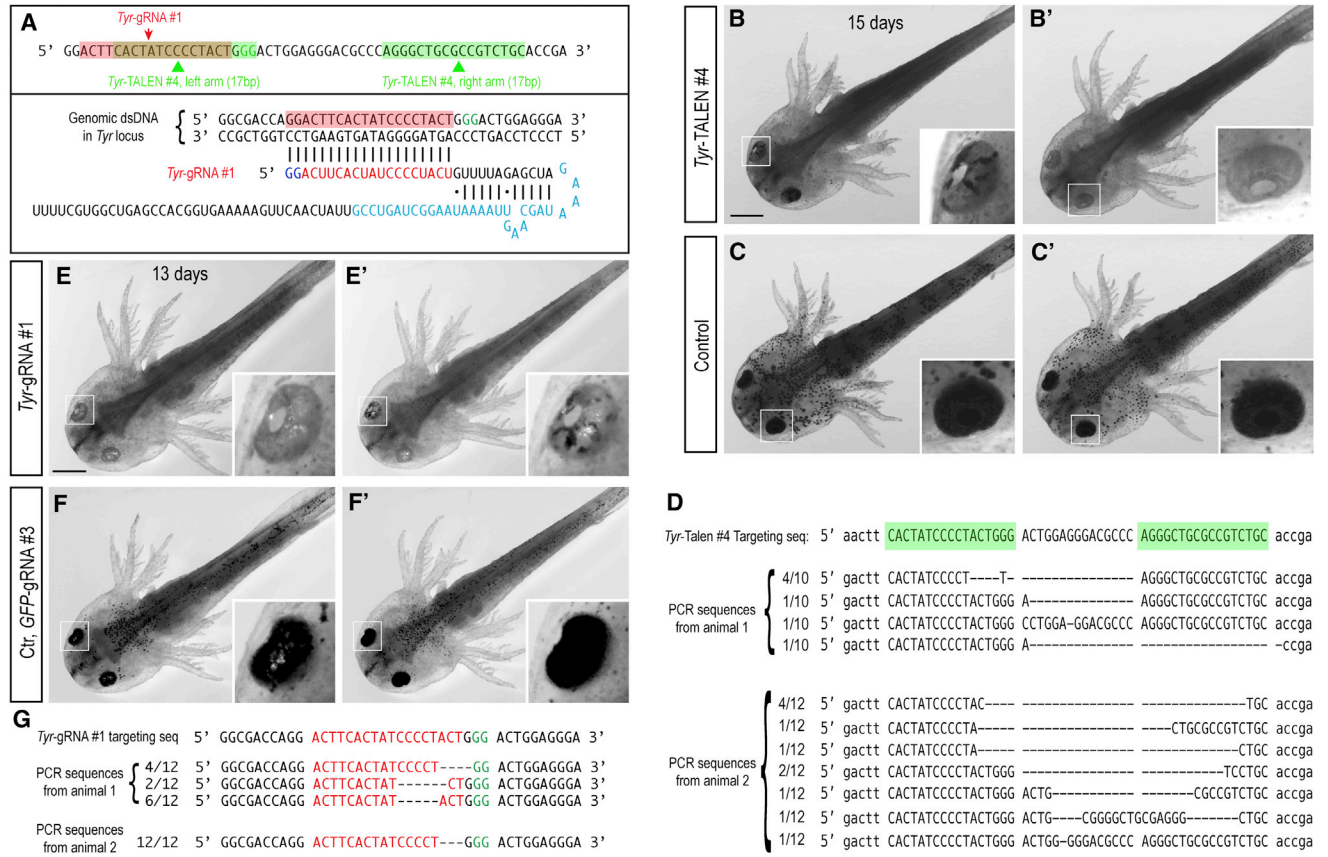
See also Tables S1–S3.

Figure 2. Deletions in the *Tyr* Gene via TALEN or CRISPR Injections

(A) TALEN and CRISPR gRNAs were designed to target the *Tyr* sequence and RNAs injected into one-cell-stage eggs.

(B and B') Two representative axolotl larva that had been injected with *Tyr*-TALEN #4 mRNAs in which >50% of cells have lost pigmentation. Scale bar, 1 mm.

(C and C') Two representative axolotl larvae injected with left-arm-only TALEN mRNAs show no loss of pigmentation.

(D) Analysis of the genomic target site in two individuals injected with *Tyr*-TALEN #4 by PCR amplification and sequencing of clones. In animal 1, seven out of ten clones showed deletions in the genomic sequence, while in animal 2, 11 out of 12 samples showed genomic modification, suggesting a high rate of modification in this animal.

(E and E') Two representative axolotl larva that had been injected with *Tyr*-gRNA#1 in which nearly all (left panel) or >50% (right panel) of cells have lost pigmentation. Scale bar, 1 mm.

(F and F') Two representative axolotl larvae injected with control *GFP*-gRNA#3 show no loss of pigmentation.

(G) Analysis of the genomic target site in two individuals injected with *Tyr*-gRNA#1 by PCR amplification and sequencing of clones. In sample 1, all (12 out of 12) clones showed deletions in the genomic sequence, while in animal 2, all (12 out of 12) samples showed the same genomic modification, suggesting that the deletion was made in the early egg/embryo.

See also Table S4.

S1C). Analysis of animals injected with *Sox2*-gRNA#4 also showed a high-penetrance *Sox2* genomic locus modification (Figure 3H). In contrast, genotyping of *Sox2*-gRNA#2-injected animals that did not show the curved-body/olfactory bulb phenotype showed only a very low frequency of gene modification (Figure S1D). These results show that animals harboring a very high penetrance of CRISPR-mediated *Sox2* deletions in the genomes of their somatic cells can survive embryonic development to day 13 larvae.

To confirm our conclusions from the CRISPR-mediated deletions, we investigated the embryonic phenotype of knocking down SOX2 protein via injection of fluorescein isothiocyanate-coupled morpholinos against the *Sox2* translational start site into one-cell-stage embryos. *Sox2* morpholino or control morpholinos were injected at three different concentrations (Figure S2A) and yielded an indistinguishable proportion of viable embryos when screened at embryonic stage 37 (Figures S2A–S2C). Immunostaining for SOX2 on cross-sections of stage 16/17

animals confirmed downregulation of SOX2 expression in *Sox2* morpholino-injected embryos (Figures S2D and S2E). The independent knockdown of SOX2 via morpholinos also revealed no detectable embryonic phenotype, confirming the results from CRISPR-mediated *Sox2* deletion.

To initially characterize the effects of SOX2 deletion in the uninjured spinal cord by immunohistochemistry, we used animals that showed approximately half-body knockout of SOX2 to have an internal control. Based on our experience with *GFP*-CRISPR knockouts, animals can often show deletion of the gene in one-half of their body, presumably due to action of the CRISPR in one of the first two blastomeres during development. When we analyzed sections of the anterior spinal cord of such animals, at least one-half of the spinal cord was lacking SOX2 expression in the cells lining the spinal cord lumen (Figure 3I). Surprisingly, in such animals, the left and right side of the spinal cord were similar in size and organization, showing NEUN$^+$ neuronal cells at the outer circumference (Figure 3I). We also observed normal expression of other markers associated with axolotl neural stem cells in the *Sox2*-deleted cells, including normal expression of GFAP and the tight junction protein ZO-1, as well as the proliferative markers proliferating cell nuclear antigen (PCNA) and phosphohistone H3 (PH3) (Figures 3J–3L). We further examined the profile of proliferation markers by injection of 5-ethynyl-2′-deoxyuridine (EdU). In the uninjured spinal cord, the incorporation of EdU was similar in the SOX2$^+$ and the SOX2$^-$ side of the spinal cord (Figure 3M).

Defective Spinal Cord Regeneration due to Lack of Enhanced Proliferation after Tail Amputation in *Sox2*-CRISPR Animals

Since the uninjured spinal cord showed normal organization under conditions of *Sox2* deletion, we went on to determine if there is a phenotype during tail regeneration. We amputated the tails of *Sox2*-CRISPR animals that showed the curved-body phenotype in order to select for animals that had a high penetrance of deletions (Figure 4A). We characterized the spinal cords in the removed portion of the tail next to the amputation plane to determine the penetrance of SOX2 deletion and the organization of the spinal cord at the starting point of the regeneration experiment. As expected, most animals showed massive or complete loss of the SOX2 spinal cord immunofluorescence signal at the amputation plane in the removed portion of the tail (Figures 4A, 4B, and S1E). Consistent with our analysis above, we found that the spinal cord size, organization, and PCNA expression was normal in spinal cords lacking SOX2$^+$ cells (Figure 4B). PCNA expression in the uninjured ependymal cells of both control and *Sox2*-CRISPR animals showed differential intensity levels that

reflect significant G1 and S phases of the slow cell cycle found in these neural stem cells under homeostatic conditions (A. Rodrigo-Albors, personal communication). We then examined whether the overall length of the regenerated spinal cord and tail was affected by following live animals at 6 and 10 days after tail amputation under oblique transillumination conditions. Animals injected with *Sox2*-gRNA#2 or with *Sox2*-gRNA#4 showed reduced or lack of spinal cord in the regenerated portion of the tail. (Figure 4C). In contrast, control *GFP*-gRNA#1-injected animals showed clear outgrowth of the spinal cord into the blastema (Figure 4C). We quantitated this phenotype by measuring the length of the overall tail regenerate versus the length of the visible spinal cord (Figure 4A). The overall tail regenerate length was unaffected in *Sox2*-CRISPR animals, while the spinal cord showed a significantly reduced length resulting in a shifted ratio of spinal cord/tail regenerate length (Figures 4D and 4E). We further correlated the extent of *Sox2* deletion found in the removed portion of the tail (see above) with the spinal cord regeneration phenotype at 6 days and found that those specimens showing complete knockout of SOX2 immunofluorescence at the amputation plane displayed the strongest spinal cord growth inhibition (Figures S1E and S1F). Analysis of the live samples at 10 days postamputation showed a continued defect in spinal cord outgrowth into the blastema (Figures S3A–S3C). By this later time point, a mild effect on blastema length was observed in some *Sox2*-deleted animals.

To characterize the spinal cord regeneration defect in more detail, we examined immunohistological sections of the spinal cord at different distances behind the amputation plane and in the regenerate at 6 and 10 days postamputation. Behind the amputation plane, in the region of the spinal cord that acts as the source zone for the regenerate (McHedlishvili et al., 2007), the spinal cord showed comparable morphology and marker expression to control animals including robust GFAP expression as well as neuron-specific tubulin, TUJ1 expression at the outer circumference (Figures 5A–5D). However, in contrast to the *Sox2*-CRISPR spinal cords that prior to amputation showed normal cell numbers (Figure 5E), in the 6- and 10-day regenerates, the number of cells per cross-section in the source zone behind the amputation plane was reduced compared to control regenerates (M1 and M2; Figures 5F and S3D). This suggests that cells from the source zone contribute to the regenerate but are not replenished. The regenerating region of the spinal cord (R1–R5; Figures 5F and S3D) showed a starkly reduced number of GFAP$^+$ spinal cord cells, especially in more distal regions of the regenerate, suggesting a defect in self-renewal and also a disorganization of TUJ1$^+$ cells (Figures 5A, 5C, and S3E). Interestingly, despite the majority of the *Sox2*-gRNA#2-injected animals showing
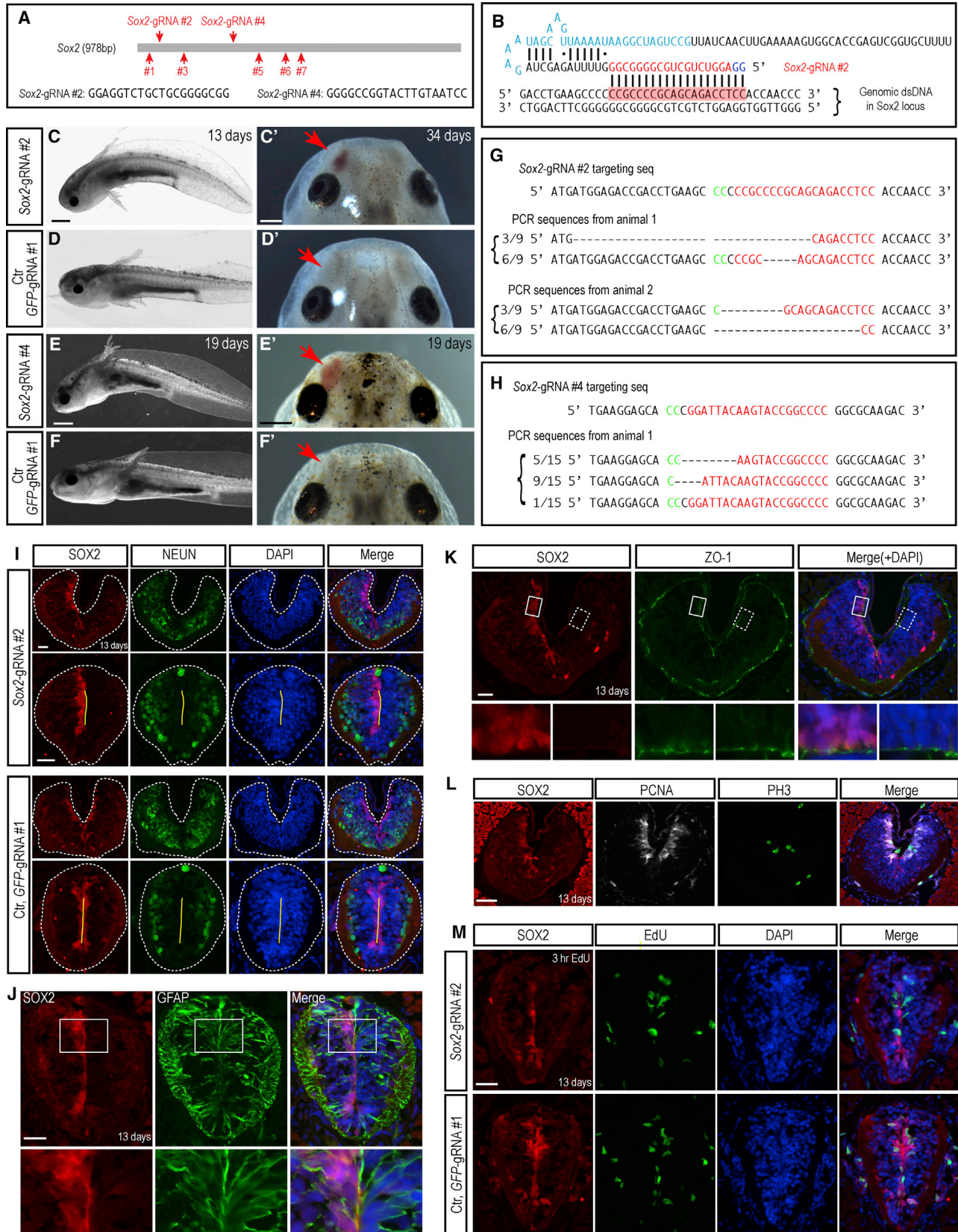
(legend on next page)

complete or nearly complete loss of SOX2 expression at the amputation plane (Figures 4B, S1C, and S1E), the regenerate routinely contained some cells that were immunopositive for SOX2. As described in *Sox2* heterozygous knockout mice, we observed specific, cytoplasmic rather than nuclear staining in some of the regenerating samples in which the few remaining SOX2+ cells seem to have contributed to the regenerated spinal cord (Avilion et al., 2003) (Figures 5C and S3E).

The above phenotype suggested that deletion of *Sox2* in neural stem cells results in a defect in proliferative expansion of neural stem cells specifically after tail amputation. To gain further insight into these proliferative properties, we first examined PCNA expression in the 6-day regenerated spinal cords. While all cells in the regenerating spinal cord of *Sox2*-CRISPR animals were positive for PCNA (Figure 6A), they showed the varying signal intensities that were more similar to the slow-cycling, nonregenerating, control spinal cord cells (Figure 4B) compared to the more homogeneous staining typical of fast-cycling neural stem cells in the control regenerates (Figure 6A). This suggested that in *Sox2*-CRISPR animals, cells do not accelerate their cell cycle efficiently and possess a significant G1 phase. To corroborate this hypothesis, we performed pulse labeling with the S phase marker EdU on regeneration day 6 for 3 hr prior to harvesting the tail for immunohistochemical processing. In the *Sox2*-CRISPR animals, we observed a marked reduction in the percentage (from 75% to 31%) of TUJ1−NEUN− spinal cord cells that incorporated EdU (Figures 6B and 6C), indicating a decreased

proliferative activity of the stem/progenitor cells. The timing or duration of the cell cycle in neural progenitors can be modulated at various phases of the cell cycle, including the Gap phases as well as S phase (Arai et al., 2011). We examined whether S phase may have slowed down in the *Sox2*-depleted cycling cells but found no evidence for a change in average EdU fluorescence intensity (Figure 6D and 6E), suggesting that the S phase properties were not altered but rather a higher percentage of cells remained in G1 or G2/M in the *Sox2*-CRISPR animals. These results indicate that lack of SOX2 results in a hampered proliferation and expansion of the neural stem/progenitor cell pool without changing a number of key markers of radial glial cell identity.

Downregulation of *Sox3* during Spinal Cord Regeneration

Considering the survival of *Sox2*-CRISPR animals through embryonic development but the strong regeneration-specific phenotype, we turned to *Sox3* as a potential family member whose expression may rationalize the *Sox2* dependence of regeneration, but not development. In frog and fish embryos, *Sox3*, whose overexpression caused expansion of the CNS and whose knockdown caused reduction of CNS tissue, was shown to control *Sox2* expression, but not vice versa (Dee et al., 2008; Rogers et al., 2009). No phenotype for *Sox2* knockdown in these models was described. *Sox2* deletion in the mouse CNS showed a mild phenotype, with a compensatory upregulation of *Sox3* (Miyagi et al., 2008). We therefore examined expression

Figure 3. Normal Spinal Cord Organization in Animals with CRISPR-Mediated Deletions in the *Sox2* Locus
(A) Schema depicting the locations of seven and sequence of two CRISPR gRNAs designed against the *Sox2* coding sequence.
(B) Schema illustrating the binding between *Sox2*-gRNA#2 and the *Sox2* target sequence.
(C–F′′) Representative axolotl larvae that received *Sox2*-gRNA#2 (C and C′) and *Sox2*-gRNA#4 (E and E′) show curved body and/or olfactory bulb defects (C′ and E′, red arrows). Animals receiving control (Ctr) *GFP*-gRNA#1 show no such defects (D, D′, F, and F′). Scale bars represent 1 mm in (C) and (E) and 0.5 mm in (C′) and (E′).
(G and H) Analysis of the genomic target site in two (G) or one (H) individuals injected with *Sox2*-gRNA#2 or *Sox2*-gRNA#4, respectively, by PCR amplification and sequencing of clones. Note: these individuals show a very high proportion of clones with modification.
(I) *Sox2*-CRISPR animals maintain normal organization of neurons. Immunofluorescence staining for SOX2 (red) and NEUN (green) combined with DAPI (blue) on spinal cord cross-sections from animals injected with *Sox2*-gRNA#2 (upper panels) or control (Ctr) *GFP*-gRNA#1. Two individual spinal cord sections along the anterior-posterior axis are shown. A significant number of *Sox2*-gRNA#2-injected animals are lacking SOX2 protein expression in at least half of the spinal cord indicating biallelic loss in one-half of the body, suggesting modification at the two-cell stage. Both SOX2+ and SOX2− sides of the spinal cord have NEUN+ neurons at the outer circumference. Dashed lines indicate spinal cord area; yellow lines indicate apical surface. Scale bars, 50 μm.
(J and K) *Sox2*-deleted cells maintain GFAP and ZO-1 expression. Immunofluorescence for SOX2 (red) and GFAP (green, J) or ZO-1 (green, K) combined with DAPI (blue) from *Sox2*-gRNA#2-injected animals. Both the side with SOX2+ cells and the side without SOX2+ cells express GFAP. Square boxes denote insets shown at higher magnification below. Scale bars, 50 μm.
(L) Normal expression of proliferative markers in *Sox2*-deleted cells. Immunofluorescence for SOX2 (red), PCNA (white), and phospho-histone H3 (green) combined with DAPI (blue) on cross-sections. Scale bar, 50 μm.
(M) Incorporation of EdU in *Sox2*-deleted cells in the uninjured spinal cord. Immunofluorescence for SOX2 (red) combined with EdU (green) and DAPI (blue) on spinal cord cross-sections from animals injected with *Sox2*-gRNA#2, with 3 hr EdU labeling before harvest. Scale bar, 50 μm.
See also Figures S1 and S2.
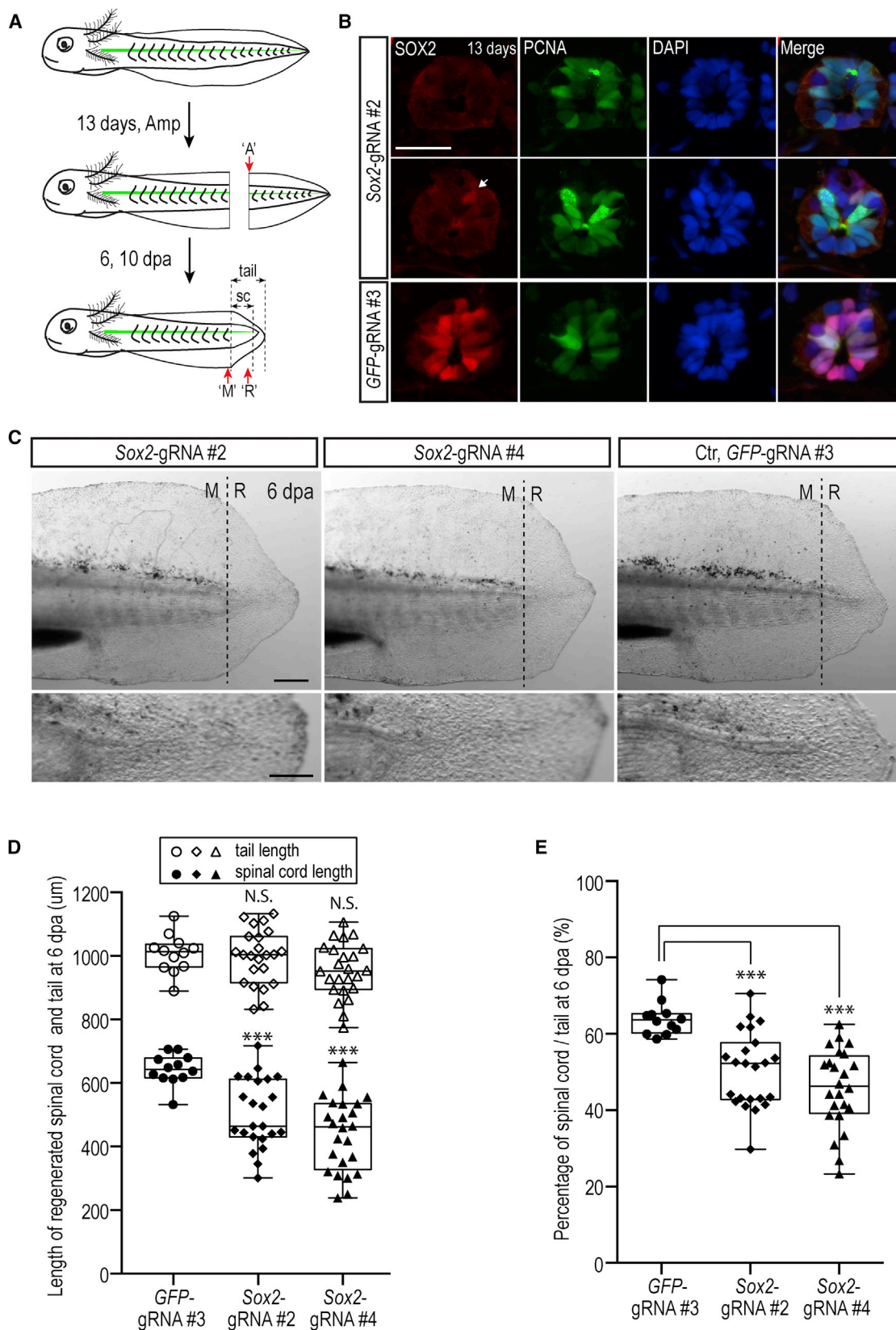
(legend on next page)

of the axolotl *Sox3* gene during development and tail regeneration. Whole-mount in situ hybridization of axolotl embryos at stages 15, 17, 34, and 37 showed indistinguishable *Sox2* and *Sox3* expression in the CNS, including the spinal cord all along the body axis (Figures 7A and 7B). This finding most likely explains the lack of embryonic phenotype in animals with reduced SOX2 either by CRISPR- or morpholino-mediated knockdown. When we checked *Sox3* expression during spinal cord regeneration by quantitative PCR and by in situ hybridization of longitudinal sections at day1 and day 6, we observed a specific downregulation of *Sox3* in the regenerating portion of the spinal cord (Figures 7C–7E). These results would correspond to a heightened sensitivity of the regenerating spinal cord to *Sox2* deletion compared to the developing spinal cord.

DISCUSSION

This work represents a number of important advances for the study of axolotl regeneration. First, we have shown for several genomic loci that TALENs and CRISPRs can induce targeted deletions in a large proportion of cells from injected animals. In all cases, CRISPRs yielded higher viability of injected animals and higher penetrance of the phenotype, reflecting deletion of both alleles within often a large majority of the cells. The *Tyr* and *Sox2* experiments show strong cellular phenotypes associated with homozygous gene deletion. In addition, for the *GFP*-transgene, we have shown germline transmission of the deletion after TALEN-mediated gene deletion. We therefore conclude that CRISPRs will be an important mode of generating gene deletions and other genome modifications in the axolotl for regeneration studies.

Our work examining CRISPR-mediated *Sox2* deletion showed mild phenotypes during development but a strong inhibition of spinal cord regeneration after tail amputation. The lack of a developmental phenotype due to SOX2 knockdown was corroborated by the injection of anti-*Sox2* morpholinos that knocked down SOX2 immunostaining in the embryo but yielded the same frequency of normally developing embryos as control-injected cohorts. It is interesting that no knockdown experiments for *Sox2* have been reported in amphibian and zebrafish embryos, raising the possibility that in these vertebrates, *Sox2* is either not solely responsible for maintenance of pluripotent cells or that maternal stores allow survival through early stages. Indeed, when we examined *Sox3*, its distribution overlapped with *Sox2* expression in the embryo, suggesting it can compensate for lack of *Sox2*, especially since *Sox3* has been shown to be upstream of *Sox2* in *Xenopus* embryos (Rogers et al., 2009). During regeneration, axolotl *Sox3* was downregulated in the spinal cord, which would be consistent with an enhanced sensitivity of the regenerate to *Sox2* knockdown.

Our analysis of tail regeneration in the *Sox2*-CRISPR animals showed that despite maintaining a number of radial glial cell markers, *Sox2*-deleted spinal cord shows defective proliferation of GFAP-positive cells and therefore, reduced outgrowth of the spinal cord at 6 and 10 days postamputation. In other work, we have defined the cell-cycle characteristics of SOX2^{+}PCNA[+]-positive cells before and after regeneration and found that in the uninjured state, resident cells cycle slowly, on average once every 14 days. Upon tail amputation, the cell cycle accelerates to a 4-day

Figure 4. Deficient Spinal Cord Regeneration in *Sox2*-CRISPR Animals
(A) Cartoon illustrates regeneration experimental scheme. Amp, amputation; dpa, day post amputation; 'A', amputated spinal cord site; 'M', mature spinal cord area; 'R', regenerated area. Dashed line indicates the amputation plane, the tip of the spinal cord, and tip of the tail.
(B) Immunofluorescence for SOX2 (red) and PCNA (green) combined with DAPI (blue) on cross-sections from the removed piece of tail just at the amputation plane ('A' in A) from animals injected with *Sox2*-gRNA#2 or *GFP*-gRNA#3. Upper and middle panels are two adjacent sections from the same animal; one shows complete loss of the SOX2-positive signal, but the other shows the presence of a single Sox2-positive cell (arrow). Scale bar, 50 μm.
(C) Images of live, 6-day regenerates. Left: *Sox2*-gRNA#2; middle: *Sox2*-gRNA#4; right: control (Ctr), *GFP*-gRNA#3. Lower panels show larger-magnification images of regenerating spinal cord area. In animals injected with *Sox2*-gRNA#2 (left lower panels) and *Sox2*-gRNA#4 (middle lower panels), a clear spinal cord tube that extends into the blastema is not visible compared to the control sample (*GFP*-gRNA#3). 'M', mature spinal cord area; 'R', regenerated area. Dashed lines represent amputation planes. Scale bars represent 500 μm in the upper panel and 200 μm in the lower panel.
(D) Quantitation of spinal cord and tail length in CRISPR *Sox2*-gRNAs versus control *GFP*-gRNA-injected animals at 6 days of regeneration. Regenerated tail length was indistinguishable between the *Sox2*-gRNA#2- (n = 23), *Sox2*-gRNA#4- (n = 24), and *GFP*-gRNA#3-injected (n = 12) animals. In contrast, *Sox2*-gRNAs-injected animals showed a significantly shorter spinal cord outgrowth. Each bullet represents one individual animal. Error bars, SD; ***p < 0.001.
(E) Spinal cord length to tail length ratio in 6-day regenerates. The spinal cord represents a smaller fraction of the total tail length in *Sox2*-gRNA-injected animals compared to controls. The same data set from (D) was used for data plotting. Each bullet represents one individual animal. Error bars, SD; ***p < 0.001.
See also Figure S3.
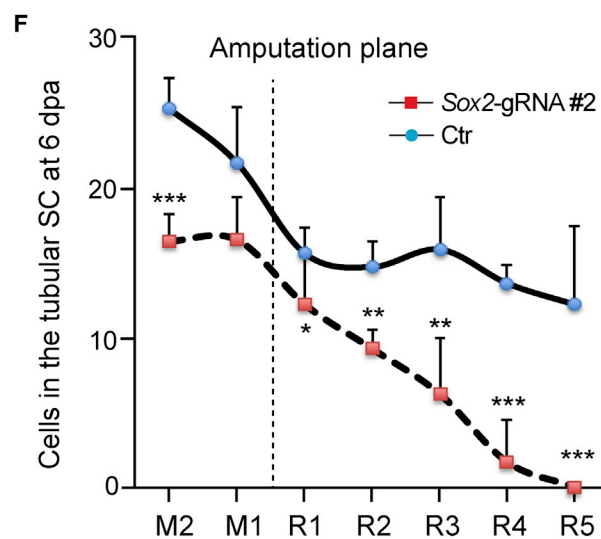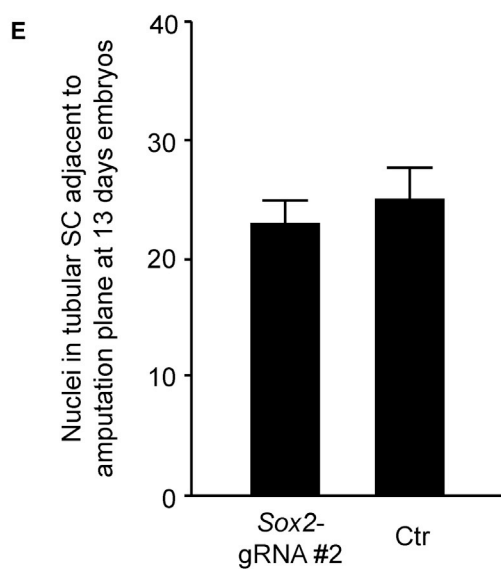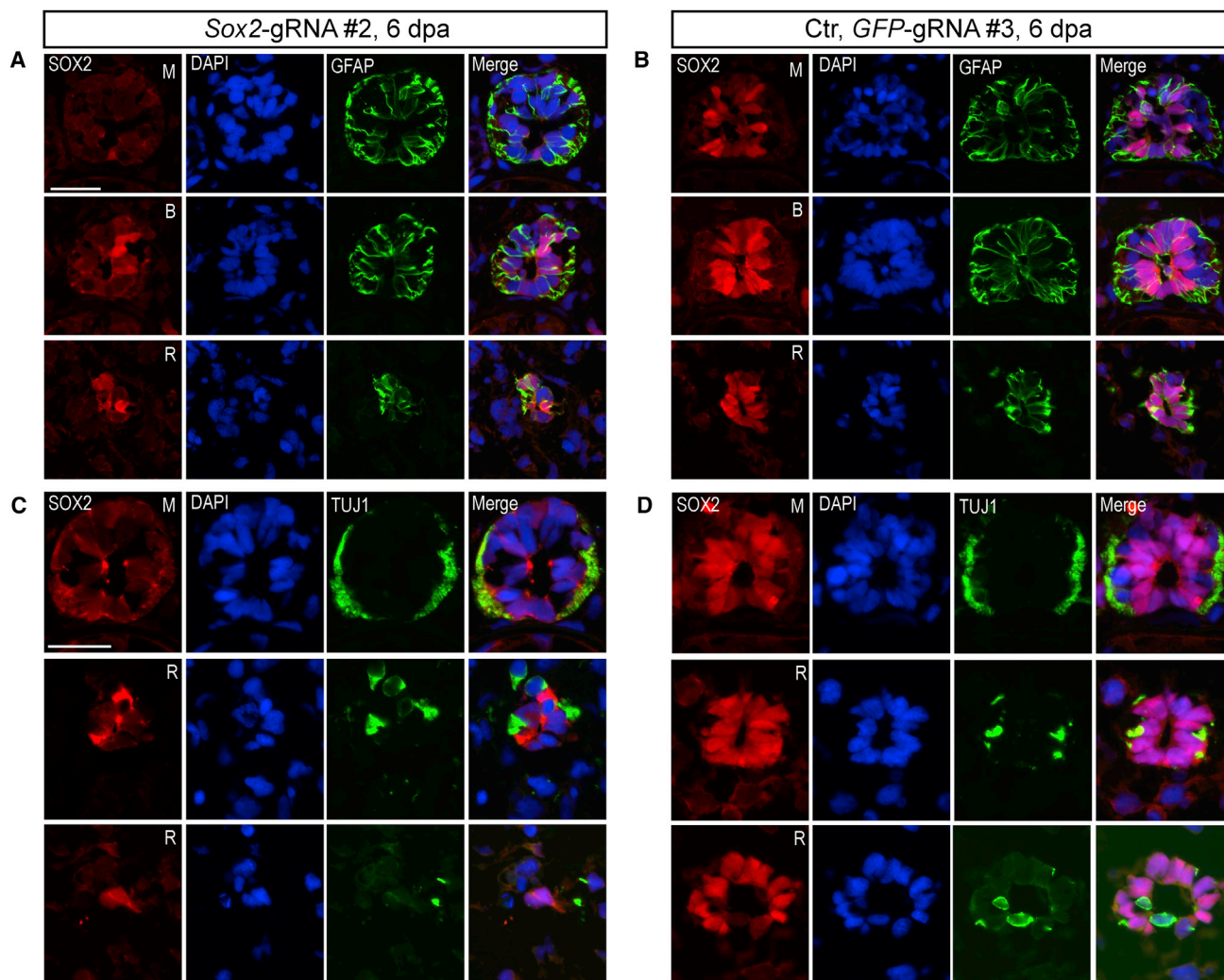
cycle (A. Rodrigo-Albors, personal communication). Given that the SOX2⁻TUJ1⁻NEUN⁻ cells at the amputation plane maintained expression of PCNA and normal levels of EdU incorporation before regeneration, we interpret this result to mean that the SOX2⁺ cells that would normally accelerate their cell cycle are, in the absence of SOX2, unable to accelerate their cell cycle in response to injury cues. The role of SOX2 in promoting proliferation of neural stem/progenitor cells has previously been documented in the brain and in CNS tumors (Favaro et al., 2009, 2014), and our work would support a role for SOX2 in injury mediated rapid cell cycles required to expand the pool of neural stem cells to reconstitute the missing spinal cord.

EXPERIMENTAL PROCEDURES

For further details, see the Supplemental Experimental Procedures. All other methods were performed according to standard protocols.

CRISPR Design and RNA Synthesis

For better comparison, relevant TALENs and CRISPRs were designed against the identical sequence of each targeted gene locus. The design and RNA synthesis were carried out according to the published protocols (Bedell et al., 2012; Cermak et al., 2011; Hwang et al., 2013).

Axolotl Care and Egg Injection

Animal experiments were carried out according to German animal welfare legislation. Axolotl egg injection was performed according to previously published protocols (Khattak et al., 2014). Briefly, 125–500 pg TALEN mRNAs, 500–1,000 pg CRISPR RNAs, or 5–20 pmol of morpholinos was injected into freshly laid single-cell-stage embryos. For TALEN- and CRISPR-mediated *GFP* knockout experiments, eggs derived from the breeding of heterozygous *GFP*-transgenic and *white* axolotl animals were used for injection. For other experiments, eggs derived from either wild-type or *white* animals were used for injection. Axolotl larvae were kept individually in plastic cups with a change of fresh tap water every second day and fed Artemia daily. Axolotl larvae were anaesthetized within 0.01% ethyl-p-aminobenzoate (benzocaine; Sigma) prior to imaging or amputation.

DNA Extraction, Genotyping, and Sequencing

Genomic DNA extraction and PCR were carried out using REDExtract-N-Amp Tissue PCR Kit (Sigma) according to the manufacturer's instructions. Each genomic locus was PCR amplified with gene-specific primer pairs (see the Supplemental Experimental Procedures). The resulting PCR products were cloned into pGEMT vector (Promega). Individual clones were sequenced with T7 primer.

Microscopy, Quantifications, and Statistics

Fluorescence images were acquired with a Zeiss Observer or confocal microscope. Bright-field or color images were acquired with an Olympus dissecting microscope. The length of the regenerated spinal cords and tails was measured with CellSens Standard software. Spinal cord cells were counted using Photoshop software. EdU⁺TUJ1⁻NEUN⁻ cells, within 300 μm of amputation plane, in the regenerated spinal cord were used for quantification in Figure 4C. EdU fluorescence intensity (in Figure 4E) was measured with Software Image J, restricted to the spinal cells expressing overall EdU (TUJ1⁻, NEUN⁻) versus epidermal cells expressing overall EdU. The punctate EdU-labeled cells were most likely excluded because they were at either the beginning or the end of S phase during EdU pulse. After subtracting the background value, the relative EdU intensity was calculated by dividing the average EdU intensity value of each individual spinal cord cell with the average EdU intensity value, minimally derived from five epidermal cells of the same section. Data plotting was carried out using Microsoft Excel and Prism. Student's t test was used for the p value calculation.

Figure 5. Cellular Analysis of Spinal Cord Regeneration defect in *Sox2*-CRISPR Animals

The defect in the regenerating spinal cord was investigated by immunofluorescence staining of cross-sections at different locations along the length of the regenerating spinal cord starting behind the amputation plane.

(A and B) Immunostaining for SOX2 (red) and GFAP (green) with DAPI shows that while the spinal cord in the mature region (M) shows similar morphology between the *Sox2*-gRNA#2- and *GFP*-gRNA#3-injected animals, in the middle region of the regeneration blastema (R), there are fewer cells in the spinal cord of the *Sox2*-gRNA#2-injected animals. Interestingly, some cells showing SOX2 staining are evident in the regenerating portion of the spinal cord. B, boundary between mature and regenerate. Scale bars, 50 μm.

(C and D) Immunostaining for SOX2 (red) and TUJ1 (green) with DAPI (blue) shows the comparable organization of neurons and axons in the mature portion of the *Sox2*-gRNA#2- and *GFP*-gRNA#3-injected animals. In contrast, the distribution of TUJ1⁺ cells is scattered and disorganized in the mid portion of the *Sox2*-gRNA#2-injected animals.

(E) Quantification of the number of nuclei in the intact spinal cord shows that *Sox2*-gRNA#2-injected animals have similar numbers of spinal cord cells to control (Ctr), *GFP*-gRNA#3-injected animals. Data are the mean value of determinants derived from four control and seven *Sox2*-gRNA#2 animals (each determinant is the average value of at least three adjacent sections close to amputation plane). Error bars, SD.

(F) Quantification of the number of nuclei in the regenerating spinal cord at different points along its length shows that cell number decreases markedly along the length of the regenerate in *Sox2*-gRNA#2-injected animals while it stays relatively constant in control *GFP*-gRNA#3-injected animals. Data are the mean value of determinants derived from four control and seven *Sox2*-gRNA#2 animals (each determinant is the average value of three sections, with 50 μm distance). Each bar on the x axis stands for 150 μm. Error bars, SD.
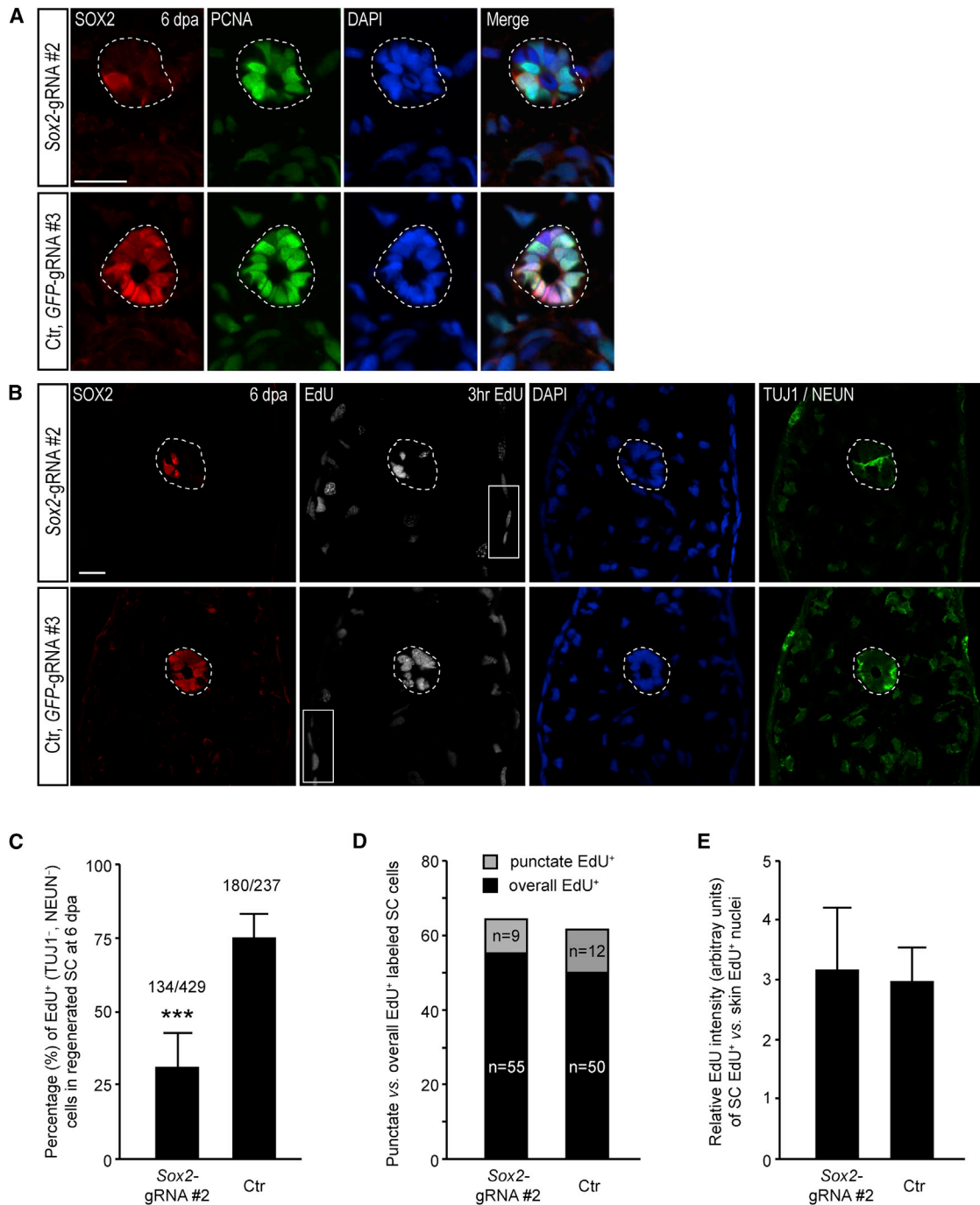
Figure 6. Reduced Proliferative Capacity of Regenerating Spinal Cord Cells in *Sox2*-CRISPR Animals

(A) Immunostaining for SOX2 (red) and PCNA (green) with DAPI (blue) shows that essentially all cells in the regenerating portion of *Sox2*-CRISPR animals at 6 dpa show PCNA staining (dotted lines). However, the heterogeneity in PCNA intensity levels more closely resembles the profile seen in an unamputated spinal cord (see Figure 4B) compared to the more uniform staining observed in a control regenerating spinal cord (Ctr). Scale bar, 50 μm.

(B) EdU incorporation was assayed to interrogate passage through the cell cycle. After a 3 hr EdU pulse, cells in the regenerating portion of the *Sox2*-gRNA#2-injected animals showed fewer EdU$^+$ cells in the spinal cord (dotted lines) compared to *GFP*-gRNA#3-injected control (Ctr) animals. In contrast, the amount of EdU incorporation in epidermis (box) was similar between the two types of animals. Scale bar, 50 μm.
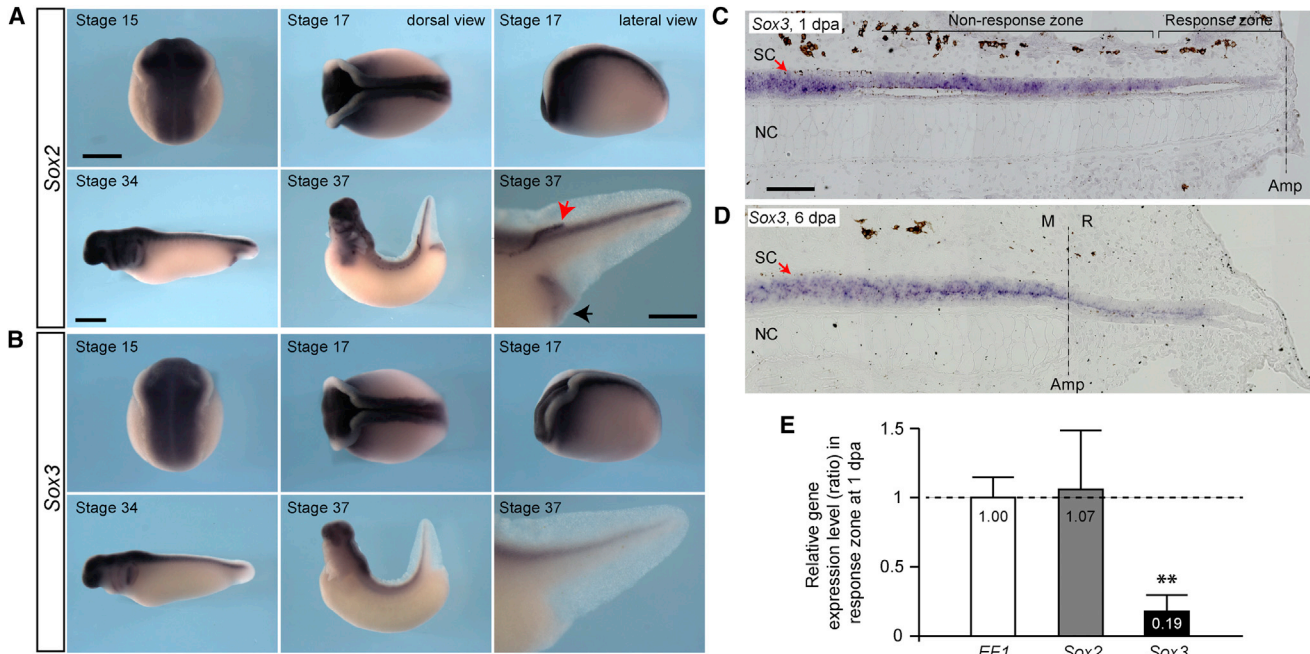
(legend continued on next page)

Figure 7. *Sox3* Expression Overlaps with *Sox2* during Development, but Not Regeneration

(A and B) *Sox2* (A) and *Sox3* (B) whole-mount in situ hybridization of axolotl embryos at stage 15, 17, 34, and 37. Note the indistinguishable *Sox2* and *Sox3* expression in the CNS, including the spinal cord, at all stages analyzed. *Sox2*, but not *Sox3*, is also expressed in the lateral line (red arrow) and cloaca (black arrow) at stage 37. Scale bars represent 1 mm in (A), left panels and 0.5 mm in (A), lower right panel.

(C) *Sox3* in situ hybridization of a 1-day regenerating tail, longitudinal section. *Sox3* expression is reduced in the 500 μm zone next to the amputation plane that will be the source of the regenerating spinal cord.

(D) *Sox3* in situ hybridization of a 6-day regenerating tail, longitudinal section. *Sox3* expression is low all along the regenerating portion of the spinal cord. SC, spinal cord; NC, nodal cord; M, mature; R, regenerate. Dashed lines represent amputation planes. Scale bar, 200 μm.

(E) Results of quantitative RT-PCR of *Sox2* and *Sox3* expression in the 500 μm response zone next to the amputation plane at 1 dpa as shown in (C) versus the 500 μm developing tail portion adjacent to the amputation plane at the day of amputation (0 dpa). Data are derived from three individual experiments and expressed as ratio of gene expression level in the response/nonresponse zone, with the ratio obtained in the case of control *EF1* being set as1 and the ratios obtained in *Sox2* and *Sox3* being expressed relative to it. Error bars, SD; **$p < 0.01$.

ACCESSION NUMBERS

The GenBank accession numbers for the *Sox2* and *Sox3* sequences reported in this paper are KJ999995 and KJ999996, respectively.

SUPPLEMENTAL INFORMATION

Supplemental Information includes Supplemental Experimental Procedures, three figures, and four tables and can be found

with this article online at http://dx.doi.org/10.1016/j.stemcr.2014.06.018.

AUTHOR CONTRIBUTIONS

J.F.F. designed, performed, and analyzed experiments and wrote the manuscript. M.S., A.T., Y.T., and K.R. performed experiments. E.M.T. provided funding, designed and analyzed experiments, and wrote the manuscript.

(C) Quantification of EdU⁺ (TUJ⁻, NEUN⁻) spinal cord cells as shown in (B) in the regenerated spinal cord within 300 μm of the amputation plane. Cells from *Sox2*-gRNA-injected animals showed a 31% incorporation rate compared to 75% in *GFP*-gRNA#3-injected control animals. In total, 429 and 237 spinal cord cells, from ten *Sox2*-gRNA#2- and four *GFP*-gRNA#3-injected control animals, respectively, were used for data plotting. Error bars, SD.

(D) Quantification of the distribution of EdU nuclear staining patterns shows that both types of animals have the same relative fraction "punctate" versus "overall" EdU label. Data derived from three *Sox2*-gRNA#2- and two *GFP*-gRNA#3-injected control animals were used for plotting.

(E) Quantification of the EdU intensity in spinal cord cells shows similar levels of incorporation, suggesting that in *Sox2*-gRNA#2-injected animals, S phase still progresses at a similar rate to controls, but more cells spend a longer time in G0, G1, or G2 phases. The "overall" EdU⁺ cells shown in (D), derived from three *Sox2*-gRNA#2- and two *GFP*-gRNA#3-injected control animals, were used for plotting. Error bars, SD.

ACKNOWLEDGMENTS

REFERENCES

Arai, Y., Pulvers, J.N., Haffner, C., Schilling, B., Nüsslein, I., Calegari, F., and Huttner, W.B. (2011). Neural stem and progenitor cells shorten S-phase on commitment to neuron production. Nat. Commun. *2*, 154.

Arnold, K., Sarkar, A., Yram, M.A., Polo, J.M., Bronson, R., Sengupta, S., Seandel, M., Geijsen, N., and Hochedlinger, K. (2011). Sox2(+) adult stem and progenitor cells are important for tissue regeneration and survival of mice. Cell Stem Cell *9*, 317–329.

Avilion, A.A., Nicolis, S.K., Pevny, L.H., Perez, L., Vivian, N., and Lovell-Badge, R. (2003). Multipotent cell lineages in early mouse development depend on SOX2 function. Genes Dev. *17*, 126–140.

Bedell, V.M., Wang, Y., Campbell, J.M., Poshusta, T.L., Starker, C.G., Krug, R.G., 2nd, Tan, W., Penheiter, S.G., Ma, A.C., Leung, A.Y., et al. (2012). In vivo genome editing using a high-efficiency TALEN system. Nature *491*, 114–118.

Blitz, I.L., Biesinger, J., Xie, X., and Cho, K.W. (2013). Biallelic genome modification in F(0) Xenopus tropicalis embryos using the CRISPR/Cas system. Genesis *51*, 827–834.

Bylund, M., Andersson, E., Novitch, B.G., and Muhr, J. (2003). Vertebrate neurogenesis is counteracted by Sox1-3 activity. Nat. Neurosci. *6*, 1162–1168.

Cermak, T., Doyle, E.L., Christian, M., Wang, L., Zhang, Y., Schmidt, C., Baller, J.A., Somia, N.V., Bogdanove, A.J., and Voytas, D.F. (2011). Efficient design and assembly of custom TALEN and other TAL effector-based constructs for DNA targeting. Nucleic Acids Res. *39*, e82.

Cong, L., Ran, F.A., Cox, D., Lin, S., Barretto, R., Habib, N., Hsu, P.D., Wu, X., Jiang, W., Marraffini, L.A., and Zhang, F. (2013). Multiplex genome engineering using CRISPR/Cas systems. Science *339*, 819–823.

Dee, C.T., Hirst, C.S., Shih, Y.H., Tripathi, V.B., Patient, R.K., and Scotting, P.J. (2008). Sox3 regulates both neural fate and differentiation in the zebrafish ectoderm. Dev. Biol. *320*, 289–301.

Echeverri, K., and Tanaka, E.M. (2005). Proximodistal patterning during limb regeneration. Dev. Biol. *279*, 391–401.

Favaro, R., Valotta, M., Ferri, A.L., Latorre, E., Mariani, J., Giachino, C., Lancini, C., Tosetti, V., Ottolenghi, S., Taylor, V., and Nicolis, S.K. (2009). Hippocampal development and neural stem cell maintenance require Sox2-dependent regulation of Shh. Nat. Neurosci. *12*, 1248–1256.

Favaro, R., Appolloni, I., Pellegatta, S., Sanga, A.B., Pagella, P., Gambini, E., Pisati, F., Ottolenghi, S., Foti, M., Finocchiaro, G., et al. (2014). Sox2 is required to maintain cancer stem cells in a mouse model of high-grade oligodendroglioma. Cancer Res. *74*, 1833–1844.

Flowers, G.P., Timberlake, A.T., McLean, K.C., Monaghan, J.R., and Crews, C.M. (2014). Highly efficient targeted mutagenesis in axolotl using Cas9 RNA-guided nuclease. Development *141*, 2165–2171.

Gaj, T., Gersbach, C.A., and Barbas, C.F., 3rd. (2013). ZFN, TALEN, and CRISPR/Cas-based methods for genome engineering. Trends Biotechnol. *31*, 397–405.

Hayashi, T., Sakamoto, K., Sakuma, T., Yokotani, N., Inoue, T., Kawaguchi, E., Agata, K., Yamamoto, T., and Takeuchi, T. (2014). Transcription activator-like effector nucleases efficiently disrupt the target gene in Iberian ribbed newts (Pleurodeles waltl), an experimental model animal for regeneration. Dev. Growth Differ. *56*, 115–121.

Hwang, W.Y., Fu, Y., Reyon, D., Maeder, M.L., Tsai, S.Q., Sander, J.D., Peterson, R.T., Yeh, J.R., and Joung, J.K. (2013). Efficient genome editing in zebrafish using a CRISPR-Cas system. Nat. Biotechnol. *31*, 227–229.

Jinek, M., Chylinski, K., Fonfara, I., Hauer, M., Doudna, J.A., and Charpentier, E. (2012). A programmable dual-RNA-guided DNA endonuclease in adaptive bacterial immunity. Science *337*, 816–821.

Kawakami, Y., Rodriguez Esteban, C., Raya, M., Kawakami, H., Martí, M., Dubova, I., and Izpisúa Belmonte, J.C. (2006). Wnt/beta-catenin signaling regulates vertebrate limb regeneration. Genes Dev. *20*, 3232–3237.

Khattak, S., Schuez, M., Richter, T., Knapp, D., Haigo, S.L., Sandoval-Guzmán, T., Hradlikova, K., Duemmler, A., Kerney, R., and Tanaka, E.M. (2013). germline transgenic methods for tracking cells and testing gene function during regeneration in the axolotl. Stem Cell Rep. *1*, 90–103.

Khattak, S., Murawala, P., Andreas, H., Kappert, V., Schuez, M., Sandoval-Guzmán, T., Crawford, K., and Tanaka, E.M. (2014). Optimized axolotl (Ambystoma mexicanum) husbandry, breeding, metamorphosis, transgenesis and tamoxifen-mediated recombination. Nat. Protoc. *9*, 529–540.

Kragl, M., Knapp, D., Nacu, E., Khattak, S., Schnapp, E., Epperlein, H.H., and Tanaka, E.M. (2008). Novel insights into the flexibility of cell and positional identity during urodele limb regeneration. Cold Spring Harb. Symp. Quant. Biol. *73*, 583–592.

Kragl, M., Knapp, D., Nacu, E., Khattak, S., Maden, M., Epperlein, H.H., and Tanaka, E.M. (2009). Cells keep a memory of their tissue origin during axolotl limb regeneration. Nature *460*, 60–65.

Lei, Y., Guo, X., Liu, Y., Cao, Y., Deng, Y., Chen, X., Cheng, C.H., Dawid, I.B., Chen, Y., and Zhao, H. (2012). Efficient targeted gene disruption in Xenopus embryos using engineered transcription activator-like effector nucleases (TALENs). Proc. Natl. Acad. Sci. USA *109*, 17484–17489.

Mali, P., Esvelt, K.M., and Church, G.M. (2013a). Cas9 as a versatile tool for engineering biology. Nat. Methods *10*, 957–963.

Mali, P., Yang, L., Esvelt, K.M., Aach, J., Guell, M., DiCarlo, J.E., Norville, J.E., and Church, G.M. (2013b). RNA-guided human genome engineering via Cas9. Science *339*, 823–826.

McHedlishvili, L., Epperlein, H.H., Telzerow, A., and Tanaka, E.M. (2007). A clonal analysis of neural progenitors during axolotl spinal cord regeneration reveals evidence for both spatially restricted and multipotent progenitors. Development *134*, 2083–2093.

McHedlishvili, L., Mazurov, V., Grassme, K.S., Goehler, K., Robl, B., Tazaki, A., Roensch, K., Duemmler, A., and Tanaka, E.M. (2012). Reconstitution of the central and peripheral nervous system during salamander tail regeneration. Proc. Natl. Acad. Sci. USA *109*, E2258–E2266.

Mercader, N., Tanaka, E.M., and Torres, M. (2005). Proximodistal identity during vertebrate limb regeneration is regulated by Meis homeodomain proteins. Development *132*, 4131–4142.

Miyagi, S., Masui, S., Niwa, H., Saito, T., Shimazaki, T., Okano, H., Nishimoto, M., Muramatsu, M., Iwama, A., and Okuda, A. (2008). Consequence of the loss of Sox2 in the developing brain of the mouse. FEBS Lett. *582*, 2811–2815.

Nakayama, T., Fish, M.B., Fisher, M., Oomen-Hajagos, J., Thomsen, G.H., and Grainger, R.M. (2013). Simple and efficient CRISPR/Cas9-mediated targeted mutagenesis in Xenopus tropicalis. Genesis *51*, 835–843.

Que, J., Luo, X., Schwartz, R.J., and Hogan, B.L. (2009). Multiple roles for Sox2 in the developing and adult mouse trachea. Development *136*, 1899–1907.

Rogers, C.D., Harafuji, N., Archer, T., Cunningham, D.D., and Casey, E.S. (2009). Xenopus Sox3 activates sox2 and geminin and indirectly represses Xvent2 expression to induce neural progenitor formation at the expense of non-neural ectodermal derivatives. Mech. Dev. *126*, 42–55.

Roy, S., Gardiner, D.M., and Bryant, S.V. (2000). Vaccinia as a tool for functional analysis in regenerating limbs: ectopic expression of Shh. Dev. Biol. *218*, 199–205.

Seifert, A.W., Kiama, S.G., Seifert, M.G., Goheen, J.R., Palmer, T.M., and Maden, M. (2012). Skin shedding and tissue regeneration in African spiny mice (Acomys). Nature *489*, 561–565.

Simon, A., and Tanaka, E.M. (2013). Limb regeneration. Wiley Interdisc. Rev. Dev. Biol. *2*, 291–300.

Sobkow, L., Epperlein, H.H., Herklotz, S., Straube, W.L., and Tanaka, E.M. (2006). A germline GFP transgenic axolotl and its use to track cell fate: dual origin of the fin mesenchyme during development and the fate of blood cells during regeneration. Dev. Biol. *290*, 386–397.

Suzuki, K.T., Isoyama, Y., Kashiwagi, K., Sakuma, T., Ochiai, H., Sakamoto, N., Furuno, N., Kashiwagi, A., and Yamamoto, T. (2013). High efficiency TALENs enable F0 functional analysis by targeted gene disruption in Xenopus laevis embryos. Biol. Open *2*, 448–452.

Takemoto, T., Uchikawa, M., Yoshida, M., Bell, D.M., Lovell-Badge, R., Papaioannou, V.E., and Kondoh, H. (2011). Tbx6-dependent Sox2 regulation determines neural or mesodermal fate in axial stem cells. Nature *470*, 394–398.

Takeo, M., Chou, W.C., Sun, Q., Lee, W., Rabbani, P., Loomis, C., Taketo, M.M., and Ito, M. (2013). Wnt activation in nail epithelium couples nail growth to digit regeneration. Nature *499*, 228–232.

Tanaka, E.M., and Ferretti, P. (2009). Considering the evolution of regeneration in the central nervous system. Nat. Rev. Neurosci. *10*, 713–723.

Tapia, N., Reinhardt, P., Duemmler, A., Wu, G., Araúzo-Bravo, M.J., Esch, D., Greber, B., Cojocaru, V., Rascon, C.A., Tazaki, A., et al. (2012). Reprogramming to pluripotency is an ancient trait of vertebrate Oct4 and Pou2 proteins. Nat. Commun. *3*, 1279.

Whited, J.L., Tsai, S.L., Beier, K.T., White, J.N., Piekarski, N., Hanken, J., Cepko, C.L., and Tabin, C.J. (2013). Pseudotyped retroviruses for infecting axolotl in vivo and in vitro. Development *140*, 1137–1146.

CRISPR-Mediated Genomic Deletion of *Sox2* in the Axolotl Shows a Requirement in Spinal Cord Neural Stem Cell Amplification during Tail Regeneration

Ji-Feng Fei, Maritta Schuez, Akira Tazaki, Yuka Taniguchi, Kathleen Roensch, and Elly M. Tanaka

Supplemental Figures and Figure Legends

Figure S1. Characterization and genotyping of *Sox2*-CRISPR animals shows a high penetrance of gene deletions even in some animals at embryonic stages. Related to Figure 3

Figure S2. Morpholino-mediated knockdown of SOX2 expression yields no detectable embryonic phenotype. Related to Figure 3

Figure S3. Analysis of the spinal cord in 10 day regenerates. Related to Figure 4

Supplemental Tables

Table S1. Embryo survival at 10 days after injection of GFP-TALEN mRNA. Related to Figure 1

Table S2. Embryo survival at 10 days after injection of GFP-CRISPR RNAs. Related to Figure 1

Table S3. Phenotype penetrance of *GFP* TALEN and CRISPR injected animals. Related to Figure1

Table S4. Phenotype penetrance of *Tyr* TALEN and CRISPR injected animals. Related to Figure 2

Supplemental Experimental Procedures

Supplemental References

Supplemental Figures and Legends

A

SOX2   13 days   DAPI   Merge

Sox2-gRNA #2

Ctr, GFP-gRNA #1
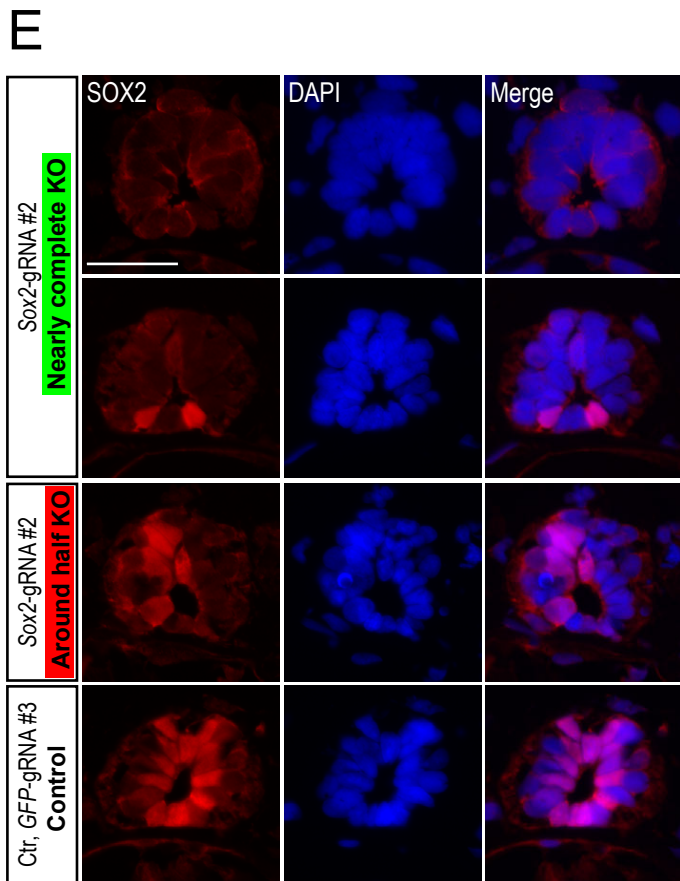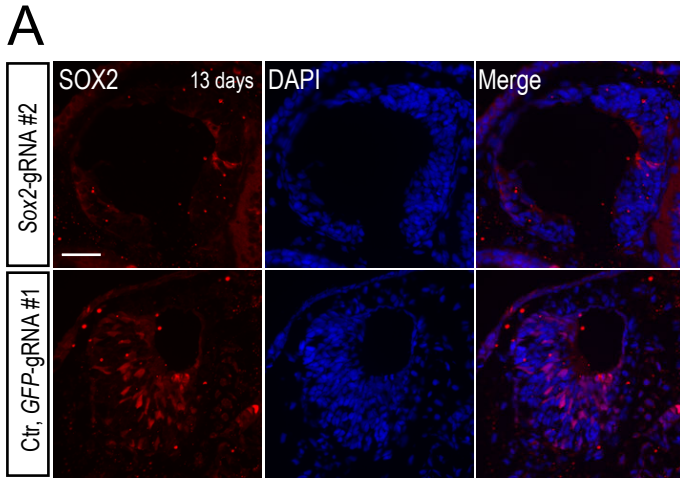
B

Sox2-gRNA#2 / Neural plate stage animals-unselected

animals #	phenotype	total clones	modified clones	percentage(%)
1	no	12	3	25
2	no	12	12	100
3	no	12	8	67
4	no	12	11	92
5	no	12	10	83
6	no	12	12	100
7	no	10	3	30
8	no	12	12	100
9	no	12	8	67
10	no	12	12	100
11	no	12	7	58

C

Sox2-gRNA#2 / 13 day animals-curved body selected

animals #	phenotype	total clones	modified clones	percentage(%)
1	curved body	10	10	100
2	curved body	11	11	100
3	curved body	12	12	100
4	curved body	12	12	100
5	curved body	12	12	100
6	curved body	12	12	100
7	curved body	9	8	89
8	curved body	12	12	100
9	curved body	11	7	64
10	curved body	10	10	100
11	curved body	12	10	83

D

Sox2-gRNA#2 / animals-no/mild phenotype selected

animals #	phenotype	total clones	modified clones	percentage(%)
1	no	10	1	10
2	no / mild	12	2	17
3	no / mild	12	1	8
4	no / mild	11	2	18

E

SOX2   DAPI   Merge

Sox2-gRNA #2 Nearly complete KO

Sox2-gRNA #2 Around half KO

Ctr, GFP-gRNA #3 Control

F

- nearly complete KO
- around half KO
- not determined

Correlation of Sox2 knockout efficiency and the length of regenerated spinal cord at 6 dpa (um)

***

GFP-gRNA #3   Sox2-gRNA #2
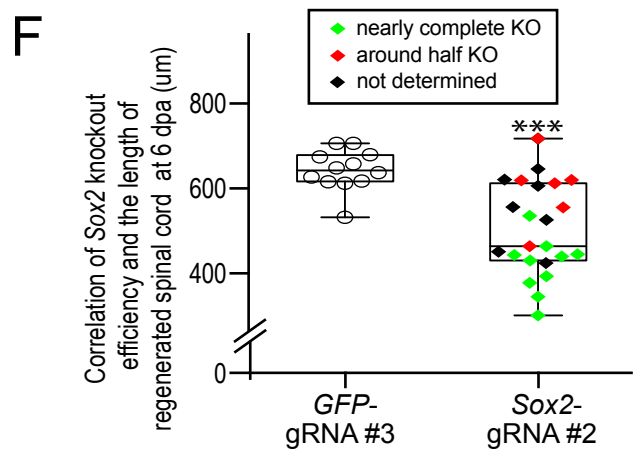
Fei et al. Supp Fig. 1

Suppl. Figure 1. Characterization and genotyping of *Sox2*-CRISPR animals shows a high penetrance of gene deletions even in some animals at embryonic stages.

A. Cross sections of the olfactory bulb from CRISPR *Sox2*-gRNA#2 versus *GFP*-gRNA#1 injected embryos were immunostained for SOX2 (red), combined with DAPI (blue). Only a few SOX2$^+$ cells are present in the *Sox2*-gRNA#2 injected animals, while controls have a number of positive cells. The pseudostratified architecture is also disrupted in the *Sox2*-gRNA#2 injected animals. Scale bar, 100μm.

B-D. Analysis of the genomic *Sox2* locus in early (B) and late (C and D) stage animals, injected with *Sox2*-gRNA#2 at single cell stage, by PCR amplification and sequencing of the clones. Note: the early stage15–neural plate stage embryos (B) used for genotyping showed normal development compared to controls and thus individuals were selected randomly for genotyping, since no phenotype could be detected yet. Late stage animals (day 13 larvae) showed either a curved body phenotype (C), or no / mild phenotype (D) and were segregated into these classes prior to genotyping. Individuals in which all clones contained deletions are highlighted in green and are present even in unselected, early stage embryos (B, 4/11). 13 day old larvae showing the curved body phenotype had a very high penetrance of deletions at the locus (C), while animals showing no / mild phenotype had a low penetrance of deletions at the locus (D) correlating the late phenotype and the genotype.

E. Categorization of SOX2 knockdown penetrance in *Sox2*-CRISPR animals used for correlating extent of *Sox2* deletion with the spinal cord regeneration phenotype in panel F. Cross sections of removed portion of the tail next to the amputation plane from *Sox2*-gRNA#2 and control *GFP*-gRNA#1 injected, 13 day old larvae (as illustrated in Fig. 4A "A", and shown in Fig. 4B) were immunostained for SOX2 (red), combined with DAPI (blue). The same animals were used later for the quantification of spinal cord and tail length at 6 days of regeneration shown in Fig. 4C-E and S1F. Note: in all the *Sox2*-gRNA#2 injected animals (upper panels), SOX2 immunostaining shows cells lacking SOX2 signal in the spinal cord compared to the control (lower panel). Green highlights animals that showed complete or nearly complete loss of SOX2 signal. Red (middle panel)

highlights animals that showed about half of the ependymal cells with loss of SOX2 prior to amputation. Scale bar, 50μm.

F. Highlighting of data in panel 4D to correlate the length of the regenerated spinal cord at 6 days with the SOX2 knockdown efficiency prior to amputation. The green and red highlighted bullets in *Sox2*-gRNA#2 samples correspond to the color categories illustrated in panel E. The green highlighted bullets that had complete or nearly complete loss of SOX2$^+$ cells in the spinal cord show a stronger spinal cord regeneration defect whereas the red highlighted bullets that had loss of around half of SOX2$^+$ cells in the spinal cord, showed a less severe spinal cord regeneration defect.

| Experiments \ Amount of Morpholino injected per egg	5 pmol	10 pmol	20 pmol
Sox2 Morpholino	17/20	18/20	17/21
Sox2 Morpholino + *Sox2* mRNA	15/21	18/21	18/21
Control Morpholino	34/40	34/40	32/39
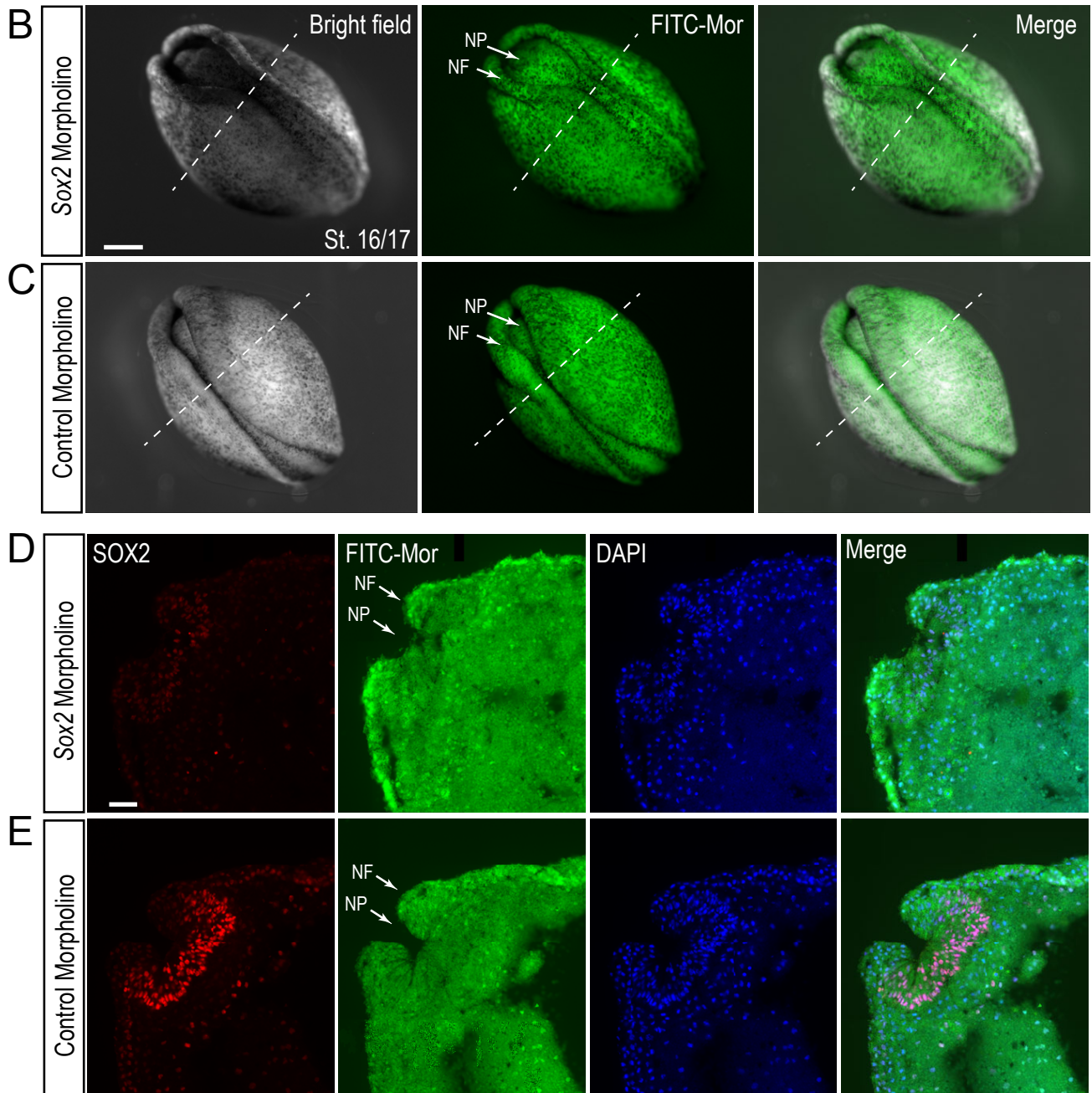
Fei et al. Supp Fig. 2

Suppl. Figure 2. Morpholino-mediated knockdown of SOX2 expression yields no detectable embryonic phenotype.

A. Embryo survival at stage 37 after injection of anti-*Sox2* Morpholinos.

B, C. Stage (St.) 16-17 axolotl embryos that had been injected at the one cell stage with 20 pmol of FITC-coupled (green) *Sox2* morpholino (B) or Control morpholino (C). NP, neural plate; NF, neural fold. Dashed lines indicate the rough positions of the cross sections in (D, E). Scale bar, 500µm.

D, E. Immunofluorescence for SOX2 (red) on cross sections of early embryos as shown in (B, C). SOX2 expression is inhibited, though not completely blocked, in *Sox2* Morpholino injected embryos. FITC-Morpholino (green), and DAPI (blue). Scale bar, 100µm.

Fei et al. Supp Fig. 3
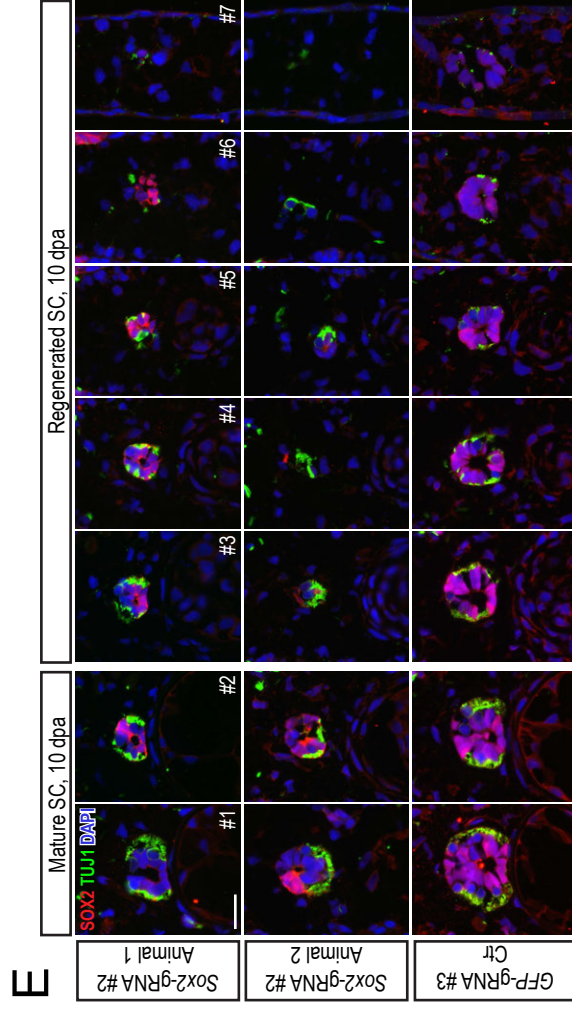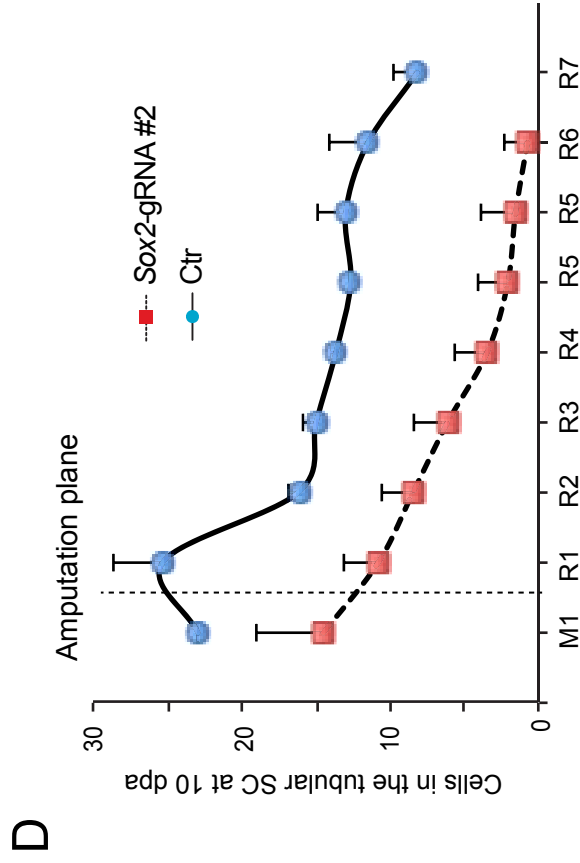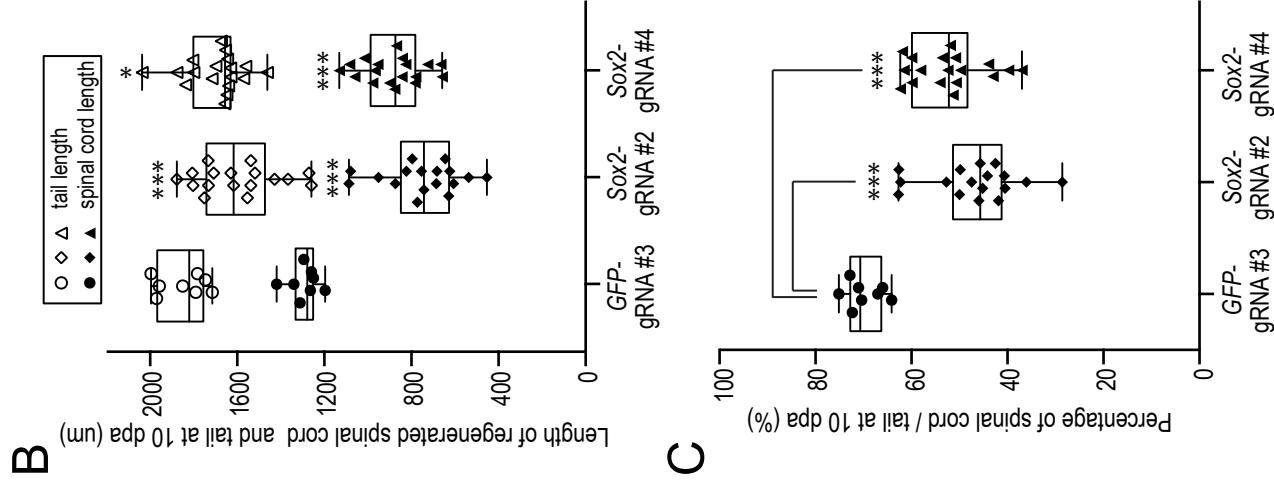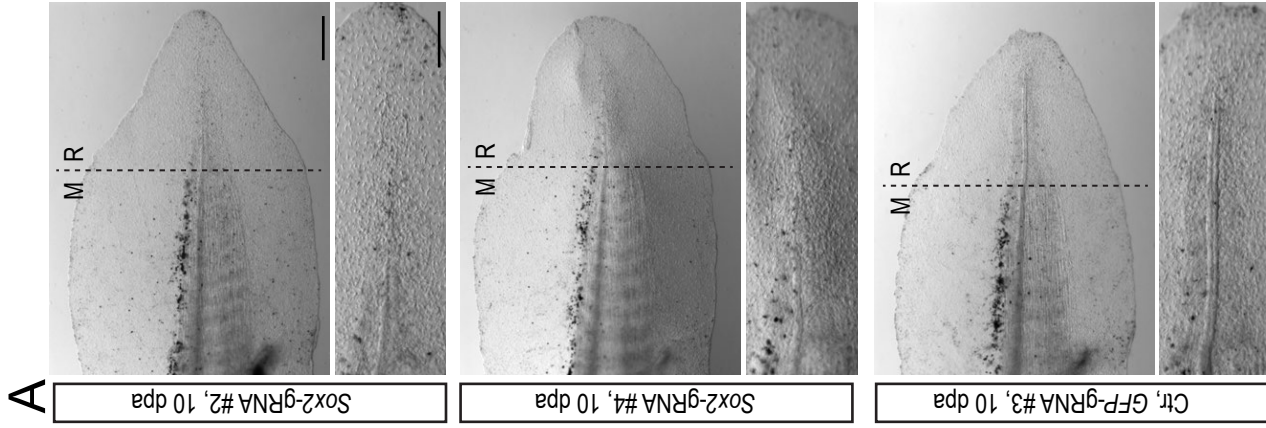
Suppl. Figure 3. Analysis of the spinal cord in 10 day regenerates.

A. Images of live, 10 day regenerates. Upper: *Sox2*-gRNA#2; middle: *Sox2*-gRNA#4 and lower: control, *GFP*-gRNA#3. Lower panels show higher magnification image of regenerating spinal cord area. In *Sox2*-gRNA#2 and *Sox2*-gRNA#4 injected animals, a clear spinal cord tube that extends into the blastema is not visible compared to the control sample (*GFP*-gRNA#3). "M", mature spinal cord area. "R", regenerated area. Dashed lines, amputation planes. Scale bars, 500μm upper panel and 200μm lower panel.

B. Quantification of spinal cord and tail length in *Sox2*-gRNAs versus control *GFP*-gRNA#3 injected animals at 10 days of regeneration. By 10 days, the regenerated tail length in *Sox2*-gRNA#2 (n=17), *Sox2*-gRNA#4 (n=18) injected animals is slightly reduced compared to control *GFP*-gRNA#3 (n=8) injected animals. The spinal cord length shows a more severe reduction in length. Each bullet means one individual animal. Error bars, SD. *$p<0.05$, ***$p<0.001$.

C. Spinal cord length to tail length ratio in 10 day regenerates. The spinal cord represents a smaller fraction of the total tail length in *Sox2*-gRNAs injected animals compared to controls. The same data set from (B) was used for data plotting. Each bullet means one individual animal. Error bars, SD; ***$p<0.001$.

D. Quantification of the number of nuclei in the spinal cord at different points along the regenerating spinal cord shows that reduced cell number along the length of the regenerate in *Sox2*-gRNA#2 injected animals compared to control *GFP*-gRNA#3 injected animals. Data are the mean of 2 determinants from control (Ctr) and 6 from *Sox2*-gRNA#2 injected animals (each determinant is the average value derived from 3 adjacent sections, with 50μm distance), Each bar on X axis stands for 150μm. Error bar in control indicate the variation of the individual values from the mean; error bar in *Sox2*-gRNA #2, SD.

E. Immunostaining for SOX2 (red) and TUJ1 (green) with DAPI (blue) shows the reduced number of cells in the spinal cord, and the disorganization of TUJ1^{+} cells in the animals injected with the *Sox2*-gRNA#2 compared to *GFP*-gRNA#3 injected animals. Sections from two different animals injected with *Sox2*-gRNA#2 are shown. From left to right, shown sections along A-P axis including mature and regenerated spinal cord (SC). Scale bar, 50μm.

Supplemental Tables

Table S1. Embryo survival at 10 days after injection of *GFP*-TALEN mRNA

[TALEN mRNA] TALEN	500pg	250pg	125pg
GFP-TALEN #1	0/44	5/50 (10%)	20/55 (36%)
GFP-TALEN #3	2/52 (4%)	21/59 (36%)	34/61 (56%)

Table S2. Embryo survival at 10 days after injection of *GFP-CRISPR* RNAs

[Cas9 mRNA] [gRNA] CRISPR gRNA	50 pg 450 pg	500 pg 500 pg	1000 pg 1000 pg
GFP-gRNA #1	92/123 (75%)	91/106 (86%)	-
GFP-gRNA #3	187/243 (77%)	58/92 (63%)	71/89 (80%)

Table S3. Phenotype penetrance of GFP TALEN and CRISPR injected animals.
"low conc." 500 pg each RNA. "high conc." 1000 pg each RNA

	Total injected eggs (50% GFP+ genotype)	Survived GFP+ genotype embryos	Phenotype: modification of GFP expression (# of animals)		
			Strong >50% loss of GFP+ cells	Weak <50% loss GFP+ cells	No visible phenotype (all GFP+)
GFP-TALEN #1	639	78	28		50
GFP-TALEN #3	871	157	40		117
Control,1L+3R	169	38	0		38
CRISPR: *GFP*-gRNA #3 low conc.	229	153	51	34	68
CRISPR: *GFP*-gRNA #3 high conc.	181	62	40	16	6
Control CRISPR: *Tyr*-gRNA #1	155	52	0	0	52

Table S4. Phenotype penetrance of *Tyr* TALEN and CRISPR injected animals.

	Total injected eggs	Survived	Phenotype: loss of pigmentation (# of animals)			
			Complete loss	Strong >90% loss	Medium >50% loss	Weak <50%
Tyr-TALEN #4	104	92	2	5	15	15
Control: *Tyr*-TALEN 3L	124	103	0	0	0	no modification
CRISPR: *Tyr*-gRNA #1	205	144	124	19	1	0
Control CRISPR: *GFP*-gRNA #3	277	219	0	0	0	no modification

Supplemental Experimental Procedures

CRISPR design and RNA synthesis

For better comparison, relevant TALENs and CRISPRs were designed against the identical sequences of each targeted gene locus. The TALENs were designed using two different programs; the 'TALEN targeter' program from Voytas'lab (Cermak et al., 2011) and the 'TALEN hit' program from the Cellectis website, with the following criteria: 17-20 RVDs in each arm of TALEN (Left or right) and 15-20 base pairs of spacer for each pair of TALEN. According to the published protocols (Bedell et al., 2012; Cermak et al., 2011), the designed TALENs were assembled into RCIscript-GoldyTALEN vector (Addgene 1000000024 and 38142), and TALEN mRNAs were synthesized using mMESSAGE mMACHINE T3 Transcription Kit (Invitrogen). According to the previous established method (Hwang et al., 2013), CRISPR gRNAs were designed using the "ZiFiT" program, and assembled into DR274 vector (Addgene 38142), then Cas9 mRNA and gRNAs were synthesized using mMESSAGE mMACHINE T7 ULTRA Transcription Kit (Invitrogen) and MAXIscript T7 Kit (Invitrogen), respectively.

List of other TALENs and CRISPR gRNA used in this study:

TALENs	Left arm sequence	Spacer	Right arm sequence
GFP-TALEN #1	CTTCAAGGACGACGGCAACT	ACAAGACCCGCGCCG	AGGTGAAGTTCGAGGGCG
GFP-TALEN #3*	TCGAGCTGGACGGCGAC	GTAAACGGCCACAAG	TTCAGCGTGTCCGGCGA
Tyr-TALEN #3	TATGCAATGCCACAGAC	GAAGGGCCCATAATA	CGTAACCCCGGCAATCA
Tyr-TALEN #4*	CACTATCCCCTACTGGG	ACTGGAGGGACGCCC	AGGGCTGCGCCGTCTGC

* corresponding sequences are also listed in the related figures.

gRNAs	gRNA sequence
GFP-gRNA #1	TGAACCGCATCGAGCTGA
GFP-gRNA #3*	CCACAAGTTCAGCGTGTC
Tyr-gRNA #1*	ACTTCACTATCCCCTACT
Tyr-gRNA #2	CGTCCCTCCAGTCCCAGT
Tyr-gRNA #3	TGCAGACGGCGCAGCCCT
Sox2-gRNA #1	TCTCCATCATGCTGTACA
Sox2-gRNA #2*	AGGTCTGCTGCGGGGCGG
Sox2-gRNA #3	CGTTGCTGCTGTTGTTGT
Sox2-gRNA #4*	ATTACAAGTACCGGCCCC
Sox2-gRNA #5	ACAAGTACACGCTGCCCG
Sox2-gRNA #6	GGTCTCCTCGGGCCACCT
Sox2-gRNA #7	GCACCGGCGGCGGCGTGG

* corresponding sequences are also listed in the related figures.

Axolotl care and egg injection

Animal experiments were carried out according to German animal welfare legislation.

Axolotl egg injection was performed according to previously published protocols (Khattak et al., 2014). Briefly, 125-500pg, typically 125pg of TALEN mRNAs (mixture of left and right arm mRNAs), CRISPR RNAs (equal mixture of 500-1000pg Cas9 mRNA and gRNA) or 5-20 pmol of FITC-coupled Morpholinos (Sox2: 5'-CGGTCTCCATCATGCTGTACATGGC-3'; Control: 5'-CCTCTTACCTCAGTTACAATTTATA-3', Gene Tools, LLC) was injected into freshly laid single-cell-stage embryos. For TALENs and CRISPR mediated GFP knockout experiments, eggs derived from the breeding of heterozygous GFP transgenic and white axolotl animals were used for injection. For other experiments, eggs derived from either wildtype or white animals were used for injection. Axolotl larvae were kept individually in plastic cups with a change of fresh tap water every

second day, and fed Artemia daily. Axolotl larvae were anaesthetized within 0.01% ethyl-p-aminobenzoate (benzocaine; Sigma) prior to imaging or amputation.

For the germ line transmission test, *GFP*-TALEN #1 and #3 injected embryos, which showed middle-high level loss of GFP expression, were raised to adulthood, and then were crossed with *white* animals. The ratio of GFP$^+$: GFP$^-$ embryos within F1 generation populations was calculated. Then genotyping and sequencing was carried out within GFP$^-$ population as described in "DNA extraction, genotyping and sequencing".

DNA extraction, genotyping and sequencing

Genomic DNA extraction and PCR were carried out using REDExtract-N-Amp™ Tissue PCR Kit (Sigma) according to the manufactory instructions. *GFP* and *Tyr* locus were PCR amplified with primer pairs *GFP*-fw & *GFP*-re and *Tyr*-fw & *Tyr*-re, respectively; *Sox2* locus were PCR amplified with *Sox2*-#2fw & *Sox2*-#2re, when injected with *Sox2*-gRNA#2, and with *Sox2*-#4fw & *Sox2*-#4re, when injected with *Sox2*-gRNA#4. The resulting PCR products were cloned into pGEMT vector (Promega). Individual clones were sequenced with T7 primer.

Genotyping PCR primers:

Primer name	Primer sequences
GFP-fw	5'-GTTCGGCTTCTGGCGTGTGAC-3'
GFP-re	5'-GCTGTTGTAGTTGTACTCCAGCTTGTGC-3'
Tyr-fw	5'-GCTCTTCCTGCTGCTCTGGGAG-3'
Tyr-re	5'-CTGCCAAGAAGCGAAGAAGGAG-3'
Sox2-#2fw	5'-GTACCTCACAAAAGACTGAAGTGAC-3'
Sox2-#2re	5'-TGCTGATCTCCGAGTTGTGCATC-3'
Sox2-#4fw	5'-ATGTACAGCATGATGGAGACCGAC-3'
Sox2-#4re	5'-GGATTCATGGAGTTGTACTGCAGG-3'

In situ hybridization

To obtain the Digoxin-labeled antisense RNA probes, the corresponding EST clones harboring

Sox2 (Genebank accession number: KJ999995) and *Sox3* (Genebank accession number:

KJ999996) coding sequences (in pCMVsports6 vector) were linearized with KpnI and EcoR1,

respectively. The probes were then synthesized using T7 RNA polymerase (Roche). Whole-mount

in situ hybridizations on albino axolotl embryos, and in situ hybridizations on 10μm longitudinal

paraffin sections, were carried out as previously described (Epperlein et al., 2000; McHedlishvili et

al., 2012).

Quantitative RT-PCR

500μm developing tail sections, measured from the amputation plane towards the tip, were

collected at the day of amputation. 500μm response zones (see Figure 7C, upper panel) of the

same animals were harvested at 1 day post amputation. Total RNA was extracted using TRIzol

reagent. qRT-PCR was performed according to the published method (Kragl et al., 2009). *EF1* was

used as internal control.

qRT-PCR primers:

Primer name	Primer sequences
EF1-RTfw	5'-CGCGAGTTCTAATAGGTTCTGATATT-3'
EF1-RTre	5'-ATGCAATTACTTTAGCGAGTACCAC-3'
Sox2-RTfw	5'-CTGCAGTACAACTCCATGAATCC-3'
Sox2-RTre	5'-ATGCTAATCATGTCCCTCAGGTC-3'
Sox3-RTfw	5'-AGGACACGCTTTGTTTATAGATGTAAT-3'
Sox3-RTre	5'-TCTGTTCTCAAGTCAAAAACAGTCTAA-3'

Immunohistochemistry

Axolotl tissue processing and immunohistochemistry were performed in according with previously

published protocols (Kragl et al., 2009). Briefly, tails or embryos were fixed overnight in 4%

MEMFA buffer, infused overnight with 30% sucrose, and then embed into OCT. 10μm cryosections were collected and stained with respective antibodies.

Microscopy, quantifications and statistics

Fluorescence images were acquired with a Zeiss Observer or confocal microscope. Bright field or color images were acquired with Olympus dissecting microscope. The length of the regenerated spinal cords and tails were measured with "CellSens Standard" software. Spinal cord cells were counted using Photoshop software. $EdU^+TUJ1^-NeuN^-$ cells, within 300μm from amputation plane, in the regenerated spinal cord were used for quantification in Figure 6C. EdU fluorescence intensity (in Figure 6E) was measured with Software Image J, restricted to the spinal cells expressing overall EdU ($TUJ1^-$, $NeuN^-$), versus epidermal expressing overall EdU. The punctate EdU labeled cells were excluded, because likely, they were at either the beginning or the end of S phase during EdU pulse. After subtracting the background value, the relative EdU intensity was calculated by dividing the average EdU intensity value of each individual spinal cells with the average EdU intensity value, minimally derived from five epidermis of the same section. Data plotting was carried out using Microsoft Excel and Prism. Student's T test was used for the p value calculation.

Supplemental References

Bedell, V.M., Wang, Y., Campbell, J.M., Poshusta, T.L., Starker, C.G., Krug, R.G., 2nd, Tan, W., Penheiter, S.G., Ma, A.C., Leung, A.Y., et al. (2012). In vivo genome editing using a high-efficiency TALEN system. Nature *491*, 114-118.

Cermak, T., Doyle, E.L., Christian, M., Wang, L., Zhang, Y., Schmidt, C., Baller, J.A., Somia, N.V., Bogdanove, A.J., and Voytas, D.F. (2011). Efficient design and assembly of custom TALEN and other TAL effector-based constructs for DNA targeting. Nucleic Acids Res. *39*, e82.

Epperlein, H., Meulemans, D., Bronner-Fraser, M., Steinbeisser, H., and Selleck, M.A. (2000). Analysis of cranial neural crest migratory pathways in axolotl using cell markers and transplantation. Development *127*, 2751-2761.

Hwang, W.Y., Fu, Y., Reyon, D., Maeder, M.L., Tsai, S.Q., Sander, J.D., Peterson, R.T., Yeh, J.R., and Joung, J.K. (2013). Efficient genome editing in zebrafish using a CRISPR-Cas system. Nat. Biotechnol. *31*, 227-229.

Khattak, S., Murawala, P., Andreas, H., Kappert, V., Schuez, M., Sandoval-Guzman, T., Crawford, K., and Tanaka, E.M. (2014). Optimized axolotl (Ambystoma mexicanum) husbandry, breeding, metamorphosis, transgenesis and tamoxifen-mediated recombination. Nat. Protoc. *9*, 529-540.

Kragl, M., Knapp, D., Nacu, E., Khattak, S., Maden, M., Epperlein, H.H., and Tanaka, E.M. (2009). Cells keep a memory of their tissue origin during axolotl limb regeneration. Nature *460*, 60-65.

McHedlishvili, L., Mazurov, V., Grassme, K.S., Goehler, K., Robl, B., Tazaki, A., Roensch, K., Duemmler, A., and Tanaka, E.M. (2012). Reconstitution of the central and peripheral nervous system during salamander tail regeneration. Proc Natl Acad Sci USA *109*, E2258-2266.